Single-spore germination analyses reveal that calcium released during *Clostridioides difficile* germination functions in a feed-forward loop.

John W. Ribis,[1,2] Luana Melo,[1] Shailab Shrestha,[1,2] David Giacalone,[1,2] Enrique E. Rodriguez, Aimee Shen[1†#], Amy Rohlfing[1,3†#]

[1]Department of Molecular Biology and Microbiology, Tufts University School of Medicine, Boston, Massachusetts, USA, [2] Graduate School of Biomedical Sciences, Tufts University School of Medicine, Boston, Massachusetts, USA.

[†]Co-corresponding authors

[3]Current address: Department of Biological Sciences, Saint Anselm College, Manchester, New Hampshire, USA

[#]Address correspondence to

Aimee Shen, aimee.shen@tufts.edu
Phone number: (617)636-3792

Amy Rohlfing, arohlfing@anselm.edu
Phone number: (603)641-7161

Abstract

Clostridioides difficile infections begin when its metabolically dormant spores germinate in response to sensing bile acid germinants alongside amino acid and divalent cation co-germinants in the small intestine. While bile acid germinants are essential for *C. difficile* spore germination, it is currently unclear whether both co-germinant signals are required. One model proposes that divalent cations, particularly Ca^{2+}, are essential for inducing germination, while another proposes that either co-germinant class can induce germination. The former model is based on the finding that spores defective in releasing large stores of internal Ca^{2+} in the form of calcium dipicolinic acid (CaDPA) cannot germinate when germination is induced with bile acid germinant and amino acid co-germinant alone. However, since the reduced optical density of CaDPA-less spores makes it difficult to accurately measure their germination, we developed a novel automated, time-lapse microscopy-based germination assay to analyze CaDPA mutant germination at the single-spore level. Using this assay, we found that CaDPA mutant spores germinate in the presence of amino acid co-germinant and bile acid germinant. Higher levels of amino acid co-germinants are nevertheless required to induce CaDPA mutant spores to germinate relative to WT spores because CaDPA released by WT spores during germination can function in a feedforward loop to potentiate the germination of other spores within the population. Collectively, these data indicate that Ca^{2+} is not essential for inducing *C. difficile* spore germination because amino acid and Ca^{2+} co-germinant signals are sensed by parallel signaling pathways.

59 **Importance**
60

61 *Clostridioides difficile* spore germination is essential for this major nosocomial pathogen to
62 initiate infection. *C. difficile* spores germinate in response to sensing bile acid germinant signals
63 alongside co-germinant signals. There are two classes of co-germinant signals: Ca^{2+} and amino
64 acids. Prior work suggested that Ca^{2+} is essential for *C. difficile* spore germination based on
65 bulk population analyses of germinating CaDPA mutant spores. Since these assays rely on
66 optical density to measure spore germination and the optical density of CaDPA mutant spores is
67 reduced relative to WT spores, this bulk assay is limited in its capacity to analyze germination.
68 To overcome this limitation, we developed an automated image analysis pipeline to monitor *C.*
69 *difficile* spore germination using time-lapse microscopy. With this analysis pipeline, we
70 demonstrate that, although Ca^{2+} is dispensable for inducing *C. difficile* spore germination,
71 CaDPA can function in a feedforward loop to potentiate the germination of neighboring spores.

Introduction

Clostridioides difficile is the leading cause of nosocomial infections and antibiotic-associated gastroenteritis worldwide. *C. difficile* causes ~450,000 infections and $5 billion dollars in associated medical costs annually in the United States (1, 2). Prior antibiotic exposure can render otherwise healthy individuals susceptible to *C. difficile* infections (CDI) because a diverse gut flora provides colonization resistance against CDI (3, 4). Once individuals become infected with *C. difficile*, they are highly susceptible to subsequent infections, with about one in five individuals experiencing at least one relapse or recurrence of CDI (2). This high incidence of repeat infections is a major contributor to CDI morbidity and mortality.

Both the vegetative and metabolically dormant spore forms of *C. difficile* contribute to the high rates of *C. difficile* disease recurrence. Vegetative *C. difficile* cells produce the glucosylating toxins, TcdA and TcdB, that induce inflammation and perpetuate gut dysbiosis (5), while its aerotolerant spores allow this obligate anaerobe to transmit disease (6). *C. difficile* spores can survive the antibiotic regimens used to treat *C. difficile* infections because they are metabolically dormant, and their resistance properties also allow them to survive exposure to commonly used disinfectants. As a result, spores serve as an environment reservoir for seeding future infections (7-10).

C. difficile infections begin when spores ingested by a susceptible individual germinate, i.e. exit dormancy, in response to specific signals sensed in the small intestine (11-13). Since germination is essential for *C. difficile* to initiate infection, its germination proteins represent promising targets for therapies designed to prevent CDI (13, 14). These proteins are likely to be selective targets because *C. difficile* uses a unique signaling pathway to initiate spore germination relative to previously characterized spore-forming bacteria such as *Bacillus subtilis* and *Clostridium perfringens* (15, 16). Almost all spore-formers use transmembrane Ger-type germinant receptors found in the inner spore membrane (17) to sense nutrient signals (e.g. amino acids and sugars) and induce germination (16, 18). In contrast, *C. difficile* is one of only two spore-formers known to lack Ger-type germinant receptors (19). Instead, *C. difficile* uses the soluble pseudoprotease CspC to sense cholate-derived bile acid germinants (20), which are found exclusively in the gastrointestinal tract of metazoans (21, 22).

Notably, bile acid germinants alone cannot induce *C. difficile* spore germination because they must be combined with co-germinant signal(s) (11). These co-germinant signals belong to two classes: amino acids and divalent cations (23, 24). Glycine is the most potent amino acid co-germinant (23, 25), and Ca^{2+} is the most potent divalent cation co-germinant (24, 26). While the chemical nature of these co-germinant signals has been well characterized, the molecular

107 mechanism by which they are physically sensed in *C. difficile* remains unclear. This is because
108 mutations in two separate genes alter co-germinant sensing. Certain mutations in the *cspBA*
109 gene, which encodes a fusion of the CspB protease to the CspA pseudoprotease (27), allow *C.*
110 *difficile* spores to germinate independent of co-germinant signals, namely in the presence of bile
111 acids alone (28). Since these mutations alter the site of interdomain processing in CspBA, which
112 changes the N-terminus of CspA (29), the CspA pseudoprotease has been proposed to function
113 as the receptor for both amino acid and Ca^{2+} co-germinants (28). While specific CspA mutations
114 allow *C. difficile* to bypass the need for co-germinants (28), specific amino acid substitutions in
115 CspC, the bile acid germinant receptor, can also alter the sensitivity of *C. difficile* spores to
116 distinct classes of co-germinants (30). These observations indicate that CspC plays a key role in
117 integrating signals from bile acid germinants *and* the two distinct co-germinant classes via an
118 unknown mechanism.
119 In response to sensing germinants and co-germinants, CspC and CspA somehow
120 activate the CspB protease (11, 13). This allows activated CspB to proteolytically activate the
121 cortex lytic enzyme, SleC (27), which then degrades the cortex, a protective layer of modified
122 peptidoglycan critical for maintaining the metabolic dormancy of spores. Degradation of the
123 cortex activates the mechanosensitive SpoVAC channel in the inner spore membrane (31-33),
124 leading to the release of large internal stores of the spore-specific small molecule, calcium
125 dipicolinic acid (CaDPA), from the spore core (34). This allows water to enter the partially
126 dehydrated spore core, leading to the resumption of metabolism and subsequent outgrowth of
127 the germinating spore into a vegetative cell.
128 Even though several proteins involved in transducing germinant and co-germinant
129 signals have been identified, there is still considerable debate regarding how *C. difficile* senses
130 the two distinct classes of co-germinant signals. Kochan *et al*. first identified that Ca^{2+} is a potent
131 co-germinant for *C. difficile* spores (24). Kochan *et al.* also showed that a CaDPA-less mutant
132 cannot germinate in the presence of bile acid germinant and amino acid co-germinant alone and
133 that the Ca^{2+} chelator, EGTA, can inhibit germination induced under these conditions (24).
134 These findings led them to propose that Ca^{2+} is absolutely required for *C. difficile* spore
135 germination, perhaps because Ca^{2+} is used as a co-factor by a key germination protein like
136 CspB (12, 24). According to this 'lock-and-key' model, the two classes of co-germinants function
137 sequentially in the same signaling pathway, but only Ca^{2+} is absolutely required as a co-
138 germinant. The alternative model is that either co-germinant class can potentiate bile acid-
139 induced germination (11, 13) such that there are parallel mechanisms for sensing the chemically
140 distinct amino acid and Ca^{2+} co-germinant signals. This model is supported by the identification

141 of specific CspC amino acid substitutions that sensitize spores to either amino acid or divalent
142 cation co-germinants (30).
143 In this study, we distinguish between these models by rigorously assessing the
144 requirement for Ca^{2+} during *C. difficile* spore germination in a panel of CaDPA-less mutant
145 spores. As CaDPA-less spores are less optically dense than spores containing CaDPA (35), it
146 can be challenging to use traditional optical density-based methods to measure the germination
147 of bulk populations. To overcome these limitations, we developed a novel time-lapse
148 microscopy-based method to simultaneously measure the germination kinetics of hundreds of
149 spores in a given experiment using automated image analysis. With this single-spore
150 germination assay, we determined that germination induced by glycine co-germinant and bile
151 acid germinant (i.e. in the absence of added Ca^{2+}) is less efficient in CaDPA-less spores relative
152 to WT. We further showed that this difference in germination behavior is because endogenous
153 Ca^{2+} released from WT spores in the form of CaDPA during germination can function in a
154 positive feedback loop to promote the germination of neighboring spores. Taken together, our
155 data strongly suggest that parallel pathways transduce signals from amino acid and Ca^{2+} co-
156 germinant classes and support a model in which CspC and CspA function in concert to integrate
157 signals from multiple environmental sources to initiate infection.
158
159
160 **Results**
161
162 **Phenotypic characterization of CaDPA mutant spores**.
163
164 The proposal that Ca^{2+} is absolutely required for *C. difficile* spore germination is largely
165 based on the finding that spores lacking CaDPA fail to germinate when germination is induced
166 by bile acid germinant taurocholate (TA) and glycine co-germinant alone (24). Since the mutant
167 spores in this study lack CaDPA due to the loss of a previously uncharacterized putative ATP-
168 binding protein, CD3298, we sought to analyze the germination phenotypes of additional
169 CaDPA mutant spores lacking known regulators of either CaDPA synthesis or transport into the
170 spore core. Namely, we deleted *dpaAB*, *spoVV*, and *spoVAC* using the *pyrE*-based allelic
171 exchange system from the 630Δ*erm*Δ*pyrE* strain background. *dpaAB* encodes the enzyme
172 complex that synthesizes CaDPA (**Fig 1A,** (35, 36)), while SpoVV and SpoVAC are critical in *B.*
173 *subtilis* for transporting CaDPA across the outer and then inner forespore membranes,
174 respectively (37, 38) (**Fig 1A**). SpoVV function was first established in *B. subtilis* (37), whereas

175 SpoVAC has been shown to transport CaDPA into the spore core in several spore-formers,
176 including *C. difficile* (32, 35, 39-43). CD3298 may act as an accessory protein for the SpoVV or
177 the SpoVAC transporter, although CD3298 lacks a signal sequence ((24), **Fig 1A**).
178
179
180
181 Consistent with prior work (24, 35), CaDPA was largely undetectable in Δ*dpaAB,*
182 Δ*spoVAC* and Δ*cd3298* spores when spores were boiled to artificially release their CaDPA
183 stores, and CaDPA was detected based on its terbium fluorescence (35, 45) (**Fig 1B**). Loss of
184 SpoVV greatly reduced CaDPA levels, although Δ*spoVV* spores contained ~5-fold higher levels
185 of CaDPA than Δ*dpaAB* mutant spores. While this difference was not statistically significant, the
186 elevated levels of CaDPA in Δ*spoVV* spores suggests that SpoVV may not be absolutely
187 required for CaDPA transport into *C. difficile* spores. Importantly, complementation of the mutant
188 strains with their respective genes from the *pyrE* locus under the control of their native
189 promoters restored CaDPA levels within the spore core (**Fig 1B**), although Δ*dpaAB*/*dpaAB*
190 spores had ~two-fold higher CaDPA levels than WT 630Δ*erm* spores (35).
191 We next compared the spore purification efficiencies of the CaDPA mutant spores. We
192 used a reduced Histodenz concentration because CaDPA mutant spores are less dense due to
193 their greater hydration (35). Consistent with our prior analyses of JIR8094 strain *dpaAB* mutant
194 spores (35), loss of DpaAB, SpoVAC, and CD3298 decreased spore purification efficiency by
195 ~two-fold (**Fig S1**), while loss of SpoVV did not affect the spore purification efficiency relative to
196 WT. The complementation strains were purified at efficiencies comparable to WT, and ~two-fold
197 more Δ*dpaAB/dpaAB* spores were isolated relative to WT, in keeping with their two-fold higher
198 levels of CaDPA relative to WT (**Fig S1**).
199 As a proxy for measuring core dehydration, we compared the intensity of our mutant
200 spores during phase-contrast microscopy analyses because spores are more "phase-bright"
201 when they are more dehydrated (35, 46, 47). By combining the MicrobeJ plug-in for ImageJ
202 (44) with manual curation to measure the intensity of individual spores by phase-contrast
203 microscopy, we found that CaDPA mutants were ~25-30% less phase-bright than WT spores;
204 Δ*CD3298* and Δ*spoVAC* spores were the least phase-bright on average (**Figs 1C, S1**).
205 Consistent with prior research indicating that core hydration is inversely correlated with
206 heat resistance (35, 48, 49), CaDPA mutant spores were highly sensitive to heat treatment (**Fig**
207 **S2**), whereas WT and complementation strain spores were resistant to 80˚C heat treatment for
208 15 minutes. Δ*spoVV* spores were the most heat-resistant of the CaDPA mutant spores tested,
209 since they maintained WT heat resistance up to 65˚C, so the small amount of CaDPA present in

210 Δ*spoVV* spores (**Fig 1B**) would appear to confer some wet heat resistance to these spores.
211 Δ*CD3298* and Δ*spoVAC* spores were the least heat-resistant, with even a 15 min treatment at
212 50˚C reducing their spore viability (**Fig S2**). The increased sensitivity of Δ*spoVAC* and Δ*CD3298*
213 spores to heat relative to *dpaAB* mutant spores suggests that CD3298 may function alongside
214 SpoVAC to transport molecules in addition to CaDPA during spore formation.
215
216 **CaDPA mutant spores appear to germinate less efficiently in optical density-based**
217 **measurements**
218
219 To assess the germination properties of CaDPA mutant spores, we used a well-
220 established germination assay to monitor their decrease in optical density over time as spores
221 degrade their cortex and hydrate their core. We previously used this assay to show that *dpaAB*
222 and *spoVAC* mutant spores decrease in optical density less than WT spores because the
223 mutant spores are more hydrated (35). Similar to these prior findings, the optical density of
224 CaDPA-less (Δ*dpaAB*, Δ*spoVAC*, and Δ*CD3298*) spores decreased less than WT spores (35%
225 vs. 50% decrease, respectively). Consistent with Δ*spoVV* spores containing some CaDPA (**Fig**
226 **1C**), the optical density decrease was Δ*spoVV* spores was intermediate between WT and
227 CaDPA-less spores (**Fig 1D**). Δ*cspC* spores exhibited no change in OD_{600} because they lack the
228 putative TA germinant receptor (20), while spores from the complementation strains exhibited
229 WT-like reductions in OD_{600} (**Fig 1D**). Notably, although the relative OD_{600} decrease in CaDPA
230 mutant spores was less than WT, their initial bulk germination rates (as defined as the average
231 OD_{600} decrease over the first 6 min of germination) in rich media containing TA germinant were
232 identical to WT irrespective of the TA concentration used. These data suggest that CaDPA
233 mutants sense germinants and hydrolyze their cortex with efficiencies similar to WT in rich
234 media containing TA germinant. These results are similar to what has been previously reported
235 for the germination response of Δ*dpaAB* spores (35) and Δ*CD3298* (24) spores in rich media
236 containing taurocholate.
237
238 **Spores lacking CaDPA do not require exogenous Ca^{2+} to germinate**
239
240 Δ*CD3298* spores were previously reported to be incapable of germinating when
241 germination is induced with TA germinant and glycine co-germinant alone (i.e. in the absence of
242 endogenous or exogenous Ca^{2+}, (24)), suggesting that Ca^{2+} is absolutely required for *C. difficile*
243 spores to germinate. To rigorously test this proposal, we compared the germination responses

244 of a panel of CaDPA mutant spores when germination is induced in the presence of TA
245 germinant and either glycine vs. Ca^{2+} co-germinant. We initially used TA germinant and co-
246 germinant concentrations that led to similar decreases in optical density as when we induced
247 germination in rich media containing 1% (19 mM) TA for WT spores (**Fig 1D**). When CaDPA
248 mutant spores were germinated in the presence of 1% (19 mM) TA and 10 mM glycine, they
249 exhibited a similar loss in optical density (**Fig 2A**) as when they were induced to germinate in
250 rich media (**Fig 1D**) or Ca^{2+} buffer containing TA germinant (**Fig 2B**). However, the initial rate at
251 which CaDPA-less spores decrease in optical density was more gradual than for WT spores,
252 especially for Δ*spoVAC* spores, indicating that CaDPA-less spores germinate more slowly as a
253 population than WT spores in the presence of 1% (19 mM) TA and 10 mM glycine (**Fig 2A**).
254 Regardless of the germinant and co-germinant concentrations used, i.e. rich media, TA +
255 glycine, or TA + Ca^{2+}, CaDPA mutant spores exhibited smaller decreases in optical density than
256 WT spores (**Fig 1C**)**.** Collectively, these results strongly suggest that Ca^{2+} is not absolutely
257 required for *C. difficile* spore germination. However, CaDPA release appears to increase the
258 average rate at which WT spores as a population germinate in response to TA germinant and
259 glycine co-germinant based on bulk optical density-based germination analyses.
260 Since these results contrasted with those of Kochan *et al.*, who failed to observe
261 Δ*CD3298* spore germination in the presence of TA and glycine co-germinant alone in OD_{600}-
262 based assays, we repeated these analyses using the same conditions employed by these
263 authors (24). Accordingly, we lowered the TA concentration to 0.2% (3.8 mM) and increased the
264 glycine concentrations to 20 and 50 mM glycine. Under these conditions, WT spores germinated
265 after a delay of ~20 min in 20 mM glycine + 0.2% (3.8 mM) TA and ~9 min in 50 mM glycine +
266 0.2% (3.8 mM) TA (**Figs 2C & D**). Although CaDPA mutant spores did not appear to germinate
267 at the lower glycine co-germinant concentration (20 mM) with 0.2% (3.8 mM) TA relative to the
268 Δ*cspC* control, their OD_{600} decreased by 10-15% after 60 min when glycine co-germinant
269 concentrations were increased to 50 mM glycine with 0.2% (3.8 mM) TA, (**Fig 2D**, $p < 0.01$).
270 Since the increased hydration of CaDPA mutant spores complicates the interpretation of
271 germination kinetics in the optical density-based assay, we analyzed germination using an
272 optical density-independent method. To this end, we assessed the proteolytic activation of the
273 cortex-degrading enzyme, SleC, by the CspB protease over time when germination was
274 induced with TA germinant and glycine co-germinant in CaDPA-less mutant spores using
275 western blotting. Under these conditions, the Δ*dpaAB* and Δ*CD3298* spores cleaved pro-SleC at
276 levels indistinguishable from WT spores and with similar kinetics (**Fig 2E**), confirming that
277 internal Ca^{2+} release is not required for *C. difficile* spores to initiate germination in the presence

278 of TA and glycine co-germinant alone. Notably, Kochan *et al*. also observed some pro-SleC
279 cleavage in Δ*cd3298* spores germinated in the presence of TA and glycine alone (24),
280 highlighting how the optical density-based germination assay has reduced sensitivity in
281 detecting germination in CaDPA mutant spores. Taken together, these data further support the
282 conclusion that Ca^{2+} is not absolutely required to induce *C. difficile* spore germination as a co-
283 germinant.
284
285 **Spores lacking CaDPA require higher levels of glycine co-germinant to germinate**
286
287 Since CaDPA mutant spores appeared to germinate more slowly than WT spores in the
288 presence of low levels of glycine co-germinant + TA germinant in the population-based optical
289 density assays (**Figs 2A-B**), CaDPA release during *C. difficile* spore germination may serve to
290 enhance TA + amino acid-induced spore germination. To directly test this possibility, we
291 compared the bulk germination rates of CaDPA mutant spores in the presence of a fixed
292 amount of TA germinant as we titrated either glycine or Ca^{2+} co-germinant. In the presence of
293 increasing concentrations of Ca^{2+} and a fixed TA concentration (0.5%, 9.5 mM), the germination
294 rate of WT spores increased steadily until it reached a maximum average rate at 7.5 mM Ca^{2+}
295 (**Figs 3A-B**). Germination rate was defined as the average change in OD_{600} in the first 6 min of
296 the assay. CaDPA mutant spores appeared to germinate at similar rates as WT spores at lower
297 Ca^{2+} concentrations; however, at 7.5 mM Ca^{2+} and above, CaDPA mutant spores appeared to
298 germinate more slowly than WT spores (**Fig 3B**). This apparent reduction in germination rate is
299 likely due to the increased hydration of CaDPA mutant spores decreasing the dynamic range of
300 the optical density-based germination assay (**Fig 3A**). Thus, CaDPA mutants would appear to
301 exhibit WT responses to Ca^{2+} co-germinant in the presence of TA germinant.
302 We next assessed how CaDPA-less spores germinate relative to WT spores when
303 germination is induced in the presence of increasing glycine co-germinant and a fixed TA
304 concentration (1%, 19 mM TA). This higher concentration of TA was needed to reliably detect
305 germination during the 60 min analysis time frame when germination was induced with TA +
306 glycine co-germinant alone. Both WT and CaDPA-less spores exhibited a lag-phase to their
307 germination, producing a sigmoidal vs. exponential decrease in OD_{600} (**Fig 3C**). Due to this lag,
308 we expanded the time frame for which we calculated the average germination rate from 0 - 15
309 minutes rather than 0 - 6 minutes. Even when germination was induced with high glycine (10
310 mM) and 1% (19 mM) TA, CaDPA mutant spores appeared to germinate more slowly relative to
311 WT (**Fig 3D**). The apparent germination rate of CaDPA mutant spores was decreased relative to

312 WT spores at all glycine co-germinant concentrations tested (**Fig 3D**). Furthermore, CaDPA
313 mutant spores required concentrations of 2.5 mM glycine to induce appreciable germination at
314 60 min in the optical density-based assay, whereas WT spore germination was detectable at 4-
315 fold lower concentrations of glycine (0.625 mM) (**Figs 3C-D**). Taken together, our data indicate
316 that CaDPA mutant spores are less sensitive to glycine co-germinant than WT spores. In
317 addition, WT spores appear to germinate more slowly as a population when germination is
318 induced in the presence of TA + glycine co-germinant compared to TA + Ca^{2+} co-germinant (**Fig**
319 **3**).
320

321 **Development of an automated image analysis pipeline for quantifying spore germination**
322 **using time-lapse microscopy**
323

324 Although the bulk germination analyses strongly suggested that internal Ca^{2+} can potentiate WT
325 spore germination, they also underscored the challenges associated with measuring the
326 germination kinetics of CaDPA mutant spores because the dynamic range of optical density-
327 based germination assays is reduced in CaDPA mutant spores because of their hydrated
328 nature. Notably, our western blot analyses of the proteolytic activation of SleC over time (**Fig**
329 **2E**) suggested that we may be missing germination events during the time frame of the OD-
330 based assays since these bulk germination assays cannot detect if a small fraction of spores
331 germinate within a population (< 5%, (51)). Furthermore, the assay can only be run for ~60-90
332 min in a plate reader because spores start to settle over time. Indeed, the OD_{600} of Δ*cspC*
333 spores decreases during this assay over time even though they are defective in inducing
334 germination, as evidenced by their constant phase-bright intensity over time ((30), **Fig 4**). It is
335 also difficult to distinguish between spores that initiate germination more slowly vs.
336 heterogeneously using bulk optical density-based assays. Since directly monitoring the
337 germination of individual spores using time-lapse microscopy would overcome many of these
338 limitations, we developed an automated time-lapse microscopy germination assay for analyzing
339 germination kinetics at the single-spore level (**Fig 4A**). When observed under phase-contrast
340 microscopy, "phase-bright" dormant spores become "phase-dark" during germination as the
341 cortex is degraded and the spore core becomes hydrated. To increase the number of spores
342 that we could analyze with this microscopy-based assay, we developed an automated image
343 analysis pipeline (PySpore) to analyze the germination of hundreds of individual spores in a
344 given field-of-view. The PySpore program allows us to determine the time to germination (T_G)
345 and the germination rates of individual spores, with T_G being defined as when spores first start

346 to decrease in phase-contrast intensity due to spore germination, and germination rate being
347 defined as the maximum absolute rate of change of a 1-D smoothing spline fitted to the mean
348 intensity of a given spore over the course of the assay. The maximum rate was calculated from
349 the first derivative of the spline which was evaluated at each timepoint (**Fig S3**).
350 While single-spore germination assays have been developed previously (52, 53),
351 developing *automated* analyses of individual germinating spores has been challenging for
352 several reasons. WT dormant spores vary in their "phase-contrast" intensity, while the intensity
353 (refractive index of the spore core) of germinating spores decreases over time as the spores
354 become more hydrated (53)). As a result, it is difficult to set a universal threshold that correctly
355 identifies all dormant spores at the start of a movie (**Fig 1C**). For example, when we tried to
356 apply SporeTracker X, a previously developed automated image analysis program developed
357 for *B. subtilis* spores (52), only ~40% of *C. difficile* spores in our movie were correctly identified
358 in the first frame (**Fig S4**).
359 To overcome the thresholding issue, we reasoned that the fixed intensity of the phase-
360 dark spore coat would allow us to segment and track spores from frame-to-frame even as the
361 intensity of their core as measured by phase-contrast microscopy changes over time during
362 germination (**Fig 4A**). By segmenting spores based on their dark outline, we were able to
363 identify >90% of spores in a given frame, improving the fidelity of spore segmentation by two-
364 fold over SporeTrackerX (**Fig S4**, (52)).
365 To validate our PySpore analysis method, we analyzed the germination of *C. difficile*
366 mutant spores with defects in cortex hydrolysis. Δ*cwlD* and Δ*pdaA* cortex modification mutants
367 degrade their cortex layer more slowly because they lack muramic-∂-lactam, a spore-specific
368 peptidoglycan modification that is recognized by the main cortex lytic enzyme, SleC (51, 54). In
369 the optical density-based bulk germination assay, Δ*cwlD* spores do not appear to germinate
370 because their OD_{600} stays largely constant, while the OD_{600} of Δ*pdaA* spores decreases slightly
371 (~10% after 3 hrs). When we analyzed the germination properties of these mutant spores on
372 agarose pads containing BHIS and 0.5% (9.5 mM) TA relative to WT spores using time-lapse
373 microscopy (**Fig 4B**), we found that a small percentage (~5%) of Δ*cwlD* spores germinated
374 during the 2 hr assay period (**Fig 4C**), with germinating spores being defined as those that
375 decrease in intensity by >20%. In contrast, ~40% of Δ*pdaA* spores germinated over the 2 hr
376 assay albeit with considerably delayed kinetics relative to WT spores. Indeed, WT spores
377 germinated rapidly and uniformly under these conditions, with most WT spores completing
378 germination within ~5 min of being exposed to germinant. In contrast, the median "time to
379 germination" for Δ*pdaA* and Δ*cwlD* spores was ~50 min (**Fig 4D**). Furthermore, these mutant

380 spores germinated more slowly at the single-spore level, with the median germination rate for a
381 given spore being ~3-fold slower than the rate measured for WT spores (**Fig 4E**). It should be
382 noted that many WT spores had already completed germination within the 2.5 min required to
383 set up a movie (**Figs 4C, 4F**), so the median germination time shown for WT spores is an
384 underestimate. Spores that had already germinated were identified by setting an intensity
385 threshold to identify phase-dark spores whose intensity did not change over the assay length
386 but had clearly completed germination. Regardless, the slower germination rate and delays in
387 time to initiation of Δ*cwlD* and Δ*pdaA* spores are consistent with their cortex modification
388 defects, which decreases the efficiency with which the SleC cortex lytic enzyme degrades the
389 unmodified cortex of these mutant spores (51, 54). Since germinant sensing is unaffected in
390 Δ*cwlD* and Δ*pdaA* spores, the delays in the "time to germination" and the slower germination
391 rates measured for these mutant spores likely reflect how both time-lapse microscopy and
392 optical density-based germination assays depend on the cortex being degraded and the core
393 becoming hydrated in order for changes in spore intensity or optical density to be detected (51,
394 54). As a result, the "time to germination" measurement reflects the initiation of germination (i.e.
395 germinant and co-germinant signal transduction), degradation of the cortex, and hydration of the
396 core. Regardless, these observations indicate that our time-lapse, single-spore germination
397 assay yields data consistent with prior optical density-based germination analyses of Δ*cwlD* and
398 Δ*pdaA* spores (51). Furthermore, the single-spore analyses (**Fig 4F**) provide additional insight
399 into the germination properties of these cortex modification mutant spores by sensitively
400 revealing their heterogeneous germination, delayed time to germination, and reduced
401 germination rate.
402
403 **Single-spore time-lapse germination analyses of Δ*dpaAB* spores reveal differences in**
404 **their germination responses to glycine vs. Ca^{2+} co-germinants**
405
406 Having established the utility of our single-spore germination assay, we next used it to analyze
407 the germination of CaDPA-less spores in the presence of TA + glycine alone (i.e. the absence
408 of added Ca^{2+}). WT and Δ*dpaAB* spores were induced to germinate in the presence of 0.2%
409 (3.8 mM) TA with 10 mM glycine. The TA concentration was lowered to 0.2% (3.8 mM) to
410 capture most of the phase-bright spores transitioning to phase-dark spores within the 2.5 min
411 needed to set up the time-lapse microscopy movies. In the presence of 0.2% (3.8 mM) TA and
412 10 mM glycine, approximately half as many Δ*dpaAB* spores germinated during the assay as WT

413 spores (**Fig 5A**), and their germination rate, as defined by the decrease in phase intensity over
414 time, was slower relative to WT (**Fig 5B**).
415 Interestingly, the germination rates measured for WT spores were more heterogenous
416 relative to Δ*dpaAB* spores, perhaps because CaDPA released from other WT spores can
417 promote the germination of neighboring spores. Consistent with this hypothesis, no difference in
418 the proportion of germinating Δ*dpaAB* and WT spores was observed over time using the single-
419 spore assay when germination was induced with 0.2% (3.8 mM) TA and 30 mM Ca^{2+} (**Fig 5A**).
420 Despite these similarities, individual Δ*dpaAB* spores still germinated more slowly than WT
421 spores, similar to our observations with TA + glycine-induced germination (**Figs 5B-C**). Again,
422 this slower apparent germination rate is likely due to the greater hydration of CaDPA mutant
423 spores, which reduces the concentration gradient between the spore core relative to the
424 surrounding media such that Δ*dpaAB* spores likely do not hydrate as quickly as WT spores.
425 Importantly, the aggregated single-spore germination data (**Fig 5C**) was similar to bulk optical
426 density-based germination analyses (**Fig S5**).
427 While these observations highlight the complexities in measuring the germination of
428 CaDPA mutant spores using phase-contrast microscopy, the single-spore germination data (i)
429 clearly demonstrate that these mutant spores can germinate in the presence of TA + glycine
430 alone, i.e. in the absence of added Ca^{2+} and (ii) suggest that internal Ca^{2+} release can
431 potentiate the germination of other spores within the population.
432
433 **Ca^{2+} released from the spore core during germination is a "public good" that can be**
434 **sensed by other spores**
435
436 To directly test the hypothesis that CaDPA released by spores can serve as a "public
437 good" to promote the germination of other spores in the population, we compared the ability of
438 germination "exudates" released from germinating WT and Δ*dpaAB* spores to induce the
439 germination of "naïve" WT spores (i.e. not previously exposed to germinant) in our time-lapse
440 microscopy assay. WT and Δ*dpaAB* spores were induced to germinate in the presence of low
441 glycine (2.5 mM) and TA (0.5%, 9.5 mM) concentrations for 16 hrs. This extended incubation
442 time was necessary to allow the population of Δ*dpaAB* spores to fully germinate, since they
443 complete germination more slowly than WT cells under these conditions (**Fig 6A**). During this
444 incubation time, WT spores release CaDPA into the supernatant fraction, while Δ*dpaAB* do not.
445 We reasoned that WT germination exudates, which contain CaDPA released by these spores,
446 would promote the germination of "naïve" WT spores more readily when incorporated into

447 agarose pads than germination exudates of Δ*dpaAB* spores, which do not contain released
448 CaDPA (**Fig 6A**). Indeed, when "naïve" WT spores were spotted onto agarose pads made from
449 WT germination exudates, a greater proportion of these spores induced germination relative to
450 spores spotted onto pads made of mock-treated buffer, which contains the 2.5 mM glycine and
451 0.5% (9.5 mM) TA originally used to prepare the WT and Δ*dpaAB* germination exudates.
452 Similarly, fewer WT spores germinated when spotted onto pads made with germination exudate
453 prepared from Δ*dpaAB* spores, which lacks CaDPA in the exudate fraction (**Fig 6B**). These
454 findings strongly suggest that CaDPA released into WT germination exudates potentiates the
455 germination of other spores in the population.
456 To more directly link the ability of WT germination exudates to promote germination to
457 the CaDPA released into these extracts, we supplemented Δ*dpaAB* germination exudates with
458 Ca^{2+} as a proxy for CaDPA (Ca^{2+} is in a one-to-one complex with DPA in the core). To match
459 the Ca^{2+} levels in WT germination exudates, we first measured the DPA concentration in WT
460 germination exudates using terbium chloride. These analyses indicated that supplementing
461 Δ*dpaAB* germination exudates with 0.2 mM calcium chloride should mimic the concentration of
462 Ca^{2+} in WT germination exudates. When 0.2 mM $CaCl_2$ was added to Δ*dpaAB* germination
463 exudates, the supplemented agarose pads rapidly induced germination in the population of WT
464 spores. Since sub-millimolar levels of Ca^{2+} were able to reduce median germination times by
465 ~3-fold, these data highlight how Ca^{2+} and glycine co-germinants can synergize to induce WT
466 spore germination, similar to a previous report by Kochan *et al*. (24). Taken together, our data
467 indicate that internal Ca^{2+} released from germinating spores potentiates the germination of other
468 spores within the population. Accordingly, CaDPA-less spores are less sensitive to glycine co-
469 germinant because they do not release CaDPA and thus cannot potentiate the germination of
470 other spores within the population.
471
472 **Ca^{2+} appears to be required for a step downstream of (co-)germinant signaling**
473
474 Although we used multiple germination analyses to demonstrate that endogenous Ca^{2+}
475 release is not necessary for germination stimulated in the presence of TA + glycine alone (Figs
476 2, 3, 5, and 6), Ca^{2+} may still be needed at low concentrations to regulate a factor required for a
477 germination step downstream of germinant and co-germinant signaling. Kochan *et al*. provided
478 evidence that Ca^{2+} may be needed as a co-factor when they showed that EGTA at a
479 concentration < 50 μM was sufficient to inhibit germination induced by 0.2% TA and 50 mM
480 glycine (Fig 2A). Addition of excess Ca^{2+} (1 mM) was sufficient to counteract the effects of

481 EGTA (Fig 2B, Kochan *et al*. 2017) and restore spore germination. Taken together, these
482 analyses with EGTA suggest that Ca^{2+} is required at concentrations < 50 μM for germination for
483 germination to proceed if Ca^{2+} serves as a co-factor.
484 In contrast, for Ca^{2+} to serve as the sole co-germinant source to promote TA-induced
485 germination, Ca^{2+} must be supplied at 2-5 mM concentrations (i.e. 100-fold higher) to function
486 as a co-germinant to promote germination at ~50% maximal levels in the presence of 0.2-0.5%
487 (3.8-9.5 mM) TA (**Fig 3B**, Kochan *et al*. 2017). However, it is also important to note that the
488 Ca^{2+} and glycine co-germinants can synergize with TA germinant such that low μM levels of
489 Ca^{2+} can stimulate germination in the presence of glycine and TA (Kochan *et al*. 2019, **Fig 6B**
490 current manuscript). As a result, it can be challenging to distinguish between the ability of Ca^{2+}
491 to potentiate germination as a co-germinant versus its requirement as a co-factor for
492 germination to proceed.
493 To attempt to distinguish between these possibilities, we titrated the Ca^{2+} chelator,
494 EGTA, to determine the minimum concentration needed to inhibit the germination of WT and
495 Δ*dpaAB* spores. For these experiments, we induced germination using the same conditions
496 used by Kochan *et al*., who previously showed that 50 μM EGTA potently inhibits WT spore
497 germination induced by 0.2% (3.8 mM) TA and 50 mM glycine (Kochan *et al*. 2017). These
498 analyses revealed that EGTA inhibited germination at concentrations between 2 and 10 μM
499 EGTA for both WT and Δ*dpaAB* spores (newly added **Fig 7A**). Interestingly, at 10 μM EGTA, we
500 observed that some WT spore preparations induced germination ~70 min into the 90 min assay,
501 suggesting that some WT spores are able to release CaDPA to sufficient levels to promote
502 germination to function in the positive feedback loop described in Fig 6. Taken together, these
503 analyses indicate that Ca^{2+} is needed at concentrations between 2-10 μM for germination to
504 proceed under the conditions tested.
505 To more directly assess whether Ca^{2+} functions as a co-germinant to stimulate
506 germination versus as a co-factor required for germination to proceed when induced by TA +
507 glycine, we compared the effect of chelating Ca^{2+} using 5 μM EGTA versus adding Ca^{2+} as a
508 co-germinant. Since we observed variation in the levels of inhibition by EGTA at 5 μM in WT
509 spores (**Fig S6**) (presumably due to the variable of endogenous Ca^{2+} release in these analyses
510 participating in a feedforward loop, Fig. 7A), we determined the effect of 5 μM EGTA vs. Ca^{2+} on
511 Δ*dpaAB* spores only. In the presence of 0.2% (3.8 mM) TA and 50 mM glycine, 5 μM EGTA
512 largely inhibited germination, while 5 μM $CaCl_2$ supplementation did not promote germination
513 above the TA + glycine alone condition (**Fig 7B**). When both 5 μM EGTA and 5 μM $CaCl_2$ were
514 added to Δ*dpaAB* spores induced to germinate in the presence of 0.2% (3.8 mM) TA and 50

515 mM glycine, $CaCl_2$ was able to partially counteract the inhibitory effect of EGTA (**Fig 7B**). Since
516 low μM concentrations of Ca^{2+} were insufficient to synergize with the glycine co-germinant
517 present in the assay, whereas equivalent concentrations of the Ca^{2+} chelator EGTA were able to
518 inhibit germination under these conditions, these results are consistent with Ca^{2+} being required
519 for a germination step downstream of germinant and co-germinant signaling. Thus, it is likely
520 that Ca^{2+} is required as a co-factor for a protein critical for germination to proceed.
521
522
523 **Discussion**
524
525 Unlike previously studied spore-formers, the nosocomial pathogen *C. difficile* requires
526 multiple environmental signals to induce germination (11, 13, 18). While *C. difficile*'s use of bile
527 acids as a germinant signal has been well-established (23), the precise requirement for amino
528 acid and divalent cation co-germinants during *C. difficile* germinant sensing has been a matter
529 of debate, with some groups proposing that divalent cations, namely Ca^{2+}, are essential for *C.*
530 *difficile* germination (24). In this study, we used a panel of CaDPA mutants and several
531 independent germination assays (optical density, single-spore, time-lapse microscopy, and
532 western blotting, **Figs 2, 4, 5**) to show that Ca^{2+} is not absolutely required as a co-germinant
533 signal for *C. difficile* spore germination. Specifically, we demonstrate that *C. difficile* mutants that
534 lack internal Ca^{2+} stores in the form of CaDPA can still germinate when exposed to bile acid and
535 amino acid co-germinants alone. However, under these conditions, CaDPA mutant spores
536 require higher concentrations of amino acid co-germinants and longer incubation times (**Figs**
537 **2,5**). While our analyses indicate that Ca^{2+} is not required as a co-germinant signal to induce
538 germination stimulated by TA + glycine alone, our analyses of germination induced by TA +
539 glycine in the presence of EGTA and/or exogenous Ca^{2+} suggest that trace levels of Ca^{2+} are
540 required for a germination step downstream of germinant sensing and signaling. Thus, Ca^{2+} is
541 likely needed as a co-factor for an enzyme required during germination (but not germinant or co-
542 germinant sensing).
543 Notably, these data indicate that *either* class of co-germinant can stimulate *C. difficile*
544 spore germination when combined with TA germinant, our findings strongly suggest that these
545 two distinct classes of co-germinants are sensed by distinct mechanisms in *C. difficile*. This
546 conclusion is supported by our prior genetic data, which identified specific substitutions in the
547 CspC bile acid germinant receptor that sensitize *C. difficile* spores to specific classes of co-
548 germinant (30). While the molecular basis for distinguishing between these distinct co-germinant

549 classes is unclear, the CspA pseudoprotease clearly plays an important role in regulating co-
550 germinant sensing given that certain CspA mutations bypass the need for either class of co-
551 germinant signals (28). Since our data indicate that parallel pathways mediate co-germinant
552 sensing, CspA may function downstream of the actual co-germinant sensor rather than as the
553 direct sensor of both classes of co-germinants. Distinguishing between these different models
554 awaits future biochemical identification of the direct sensors of amino acids and Ca^{2+},
555 respectively. Regardless, our data suggest that distinct regions of the same receptor or two
556 distinct receptors are involved in sensing amino acid and Ca^{2+} co-germinant signals,
557 respectively.

558 Notably, rigorously assessing the requirement for Ca^{2+} as a co-germinant signal during
559 *C. difficile* spore germination required that we optimize a method for directly monitoring spore
560 germination at the single-cell level (**Fig 3**). This method was necessary because the lack of
561 CaDPA in these mutant spores made it difficult to use traditional optical density-based assays to
562 accurately monitor their germination over time. By coupling time-lapse microscopy analyses of
563 individual spores to our custom image analysis pipeline (**Fig 4**), we were able to demonstrate
564 that CaDPA-less spores still germinate when germination is induced by TA + glycine alone, i.e.
565 in the absence of added Ca^{2+}, although a smaller fraction of Δ*dpaAB* spores germinated under
566 these conditions relative to WT or to Δ*dpaAB* spores germinated with taurocholate and calcium
567 (**Fig 4**), highlighting how CaDPA release can potentiate germination of other spores within the
568 population. Indeed, our germination exudate experiments allowed us to demonstrate that
569 CaDPA released during *C. difficile* spore germination forms a feedforward loop that potentiates
570 the germination of neighboring spores when germination is induced by TA and amino acid
571 germinants alone (**Fig 5**). While the physiological significance of this feedforward loop remains
572 unclear, it is possible that local changes in Ca^{2+} within the gut could promote *C. difficile* spore
573 germination, especially glycine was recently shown to be a limiting factor for establishing
574 infection (55). Indeed, it is possible that spores from other bacterial species could potentiate *C.*
575 *difficile* spore germination, since CaDPA is released by all germinating spores. Unfortunately,
576 testing whether CaDPA release by neighboring spores contributes to germination *in vivo* could
577 be challenging given that CaDPA-less spores have decreased resistance properties and may
578 not survive passage through the stomach.

579 Our analyses of several strains with CaDPA defects also provide new insight into how
580 CaDPA is incorporated into *C. difficile* spores. Our data confirm that SpoVV regulates CaDPA
581 transport in *C. difficile* likely by allowing CaDPA to cross the mother cell-derived outer forespore
582 membrane as previously shown in *B. subtilis* (37). However, in contrast with *B. subtilis*, some

583 CaDPA can still be transported into *C. difficile* spores in the absence of SpoVV, implying that
584 there is an additional transporter that can partially substitute the loss of its function. In addition,
585 our data suggest that CD3298, a putative ATP-binding protein, regulates SpoVAC function,
586 since the resistance and germination phenotypes of Δ*cd3298* spores most closely resemble
587 those of Δ*spoVAC* spores. Alternatively, CD3298 may work in concert with SpoVV and the
588 unidentified alternative CaDPA transporter located in the mother cell-derived outer forespore
589 membrane.
590 Taken together, our findings resolve an important question in our understanding of how
591 *C. difficile* integrates signals from amino acid and Ca^{2+} co-germinants alongside bile acid
592 germinants by demonstrating that either co-germinant class is sufficient to function as a co-
593 germinant. They also provide a new quantitative method for monitoring germination kinetics
594 over time, since our automated PySpore method allows the germination of hundreds to
595 thousands of spores to be analyzed over time. Since this method is not specific to *C. difficile*, it
596 can be applied to study mechanisms of germination initiation and germination heterogeneity in
597 other spore-formers with greater accuracy than existing programs (**Fig S4**). The ease with which
598 this program can be implemented by other investigators and its improved accuracy in identifying
599 spores within a population will hopefully allow the method to be adopted more widely.
600
601
602
603 **Materials and Methods**
604
605 **Bacterial strains and growth conditions**
606 The parental strain for all *C. difficile* strains in the study was 630Δ*erm*Δ*pyrE*. Allele coupled
607 exchange (ACE), which allows for in-frame gene deletions and complementation in an ectopic
608 locus, was used to generate all strains (56). *C. difficile* strains are listed in **Table S1** were grown
609 on brain heart infusion (BHI) media supplemented with L-cysteine (0.1% w/v; 8.25 mM),
610 taurocholate (TA, 0.1% w/v, 1.9 mM), thiamphenicol (5-15 µg/mL), kanamycin (50 µgmL) or
611 cefoxitin (8 µg/mL), as needed. For constructing in-frame deletions using allele coupled
612 exchange, *C. difficile* defined media (CDDM, (57)) was supplemented with 5-flouroorotic acid (5-
613 FOA, 2 mg/mL) and uracil (5 µg/mL). Cultures were grown at 37˚C under anaerobic conditions
614 using a gas mixture containing 85% N_2, 5% CO_2 and 5-10% H_2.
615
616 *Escherichia coli* DH5α strain was used for all plasmid construction and *E. coli* strain
617 HB101/pRK24 was used for conjugating plasmids for ACE into *C. difficile*. All HB101 strains
618 used in this study are listed in **Table S1**. E. *coli* strains were grown in Luria-Bertani broth (LB) at

619 37˚C with shaking at 225 rpm. The media was supplemented with chloramphenicol (20 µg/mL)
620 or ampicillin (50 µg/mL) as indicated.
621
622 ***E. coli* strain construction**
623 Plasmid constructs were cloned into DH5α strains and sequenced confirmed using Genewiz
624 Sanger sequencing. Benchling plasmid maps for all constructs and primers used in strain
625 construction are included in **Table S2**. PCR products were cloned into pMTL-YN3 digested with
626 AscI and Sbf1 or pMTL-YN1C digested with NotI and XhoI using Gibson assembly. Sequenced
627 confirmed plasmids were then cloned into HB101 strains to conjugate into *C. difficile* strains.
628
629 ***C. difficile* strain construction**
630 *C. difficile* in-frame deletions strains were generated with ACE by conjugating pMTL-YN3
631 plasmid constructs in HB101 into the 630Δ*erm*Δ*pryE* parental strain. Deletions were confirmed
632 by diagnostic PCR and two individual clones were phenotypically characterized before restoring
633 the *pyrE* locus. The *pyrE* locus was restored with ACE by conjugating the pMTL-YN1C plasmid
634 into the deletion strain or through complementation with appropriate pMTL-YN1C plasmid
635 containing the gene of interest. Two individual complementation clones were phenotypically
636 characterized. All strains used for conjugations are included in Table S1.
637
638 **Spore purification**
639 Strains were grown on 70:30 agar media for 2-3 days to induce sporulation as previously
640 described (58). Cultures were harvested into ice-cold, sterile water. Spore samples were
641 washed 5-6 times in ice-cold, sterile water and incubated overnight in sterile water at 4˚C. After
642 incubation, spore solutions were washed in ice-cold, sterile water and then treated with DNase I
643 (New England Biolabs) for 60 mins at 37˚C. Spores were then purified on a 20%/45% Histodenz
644 (Sigma Aldrich) gradient. The 45% Histodenz was required to isolate the less dense, CaDPA-
645 less spores (35). The resulting spores were washed 2 times in ice-cold, sterile water and
646 assessed for purity using phase-contrast microscopy. Spore stocks were stored at 4˚C in sterile
647 water. OD_{600} of the spore stock was measured as a proxy for spore concentration. The average
648 spore purification yield per agarose plate was determined from three independent spore
649 purifications.
650
651 **Total DPA quantification using terbium fluorescence**

652 The total DPA content of spores were measured using terbium fluorescence essentially as
653 described in (35). The equivalent 0.35 OD_{600} units of spores, or ~1 x 10^7 spores, were
654 suspended in 500 µL spore lysis buffer (0.3 mM $(NH_4)_2SO_4$, 6.6 mM KH_2PO_4, 15 mM NaCl, 59.5
655 mM $NaHCO_3$, 35.2 mM Na_2HPO_4). Spores in lysis buffer were split into two tubes, with one set
656 being incubated at 37˚C for 1 hour (untreated control) and the other set at 95˚C for 1 hour.
657 Samples were spun at 15,000 rpm for 2 minutes. 10 µL of supernatant was added to 115 µL of
658 10 mM Tris, 150 mM NaCl buffer with 800 µM terbium chloride in a black 96-well plate. Boiled
659 WT spore supernatant was added to 10 mM Tris, 150 mM NaCl buffer without terbium chloride
660 to determine background fluorescence. The fluorescence of terbium chloride (45) was
661 measured in a Synergy H1 microplate reader (Biotek; excitation: 270 nm, emission: 545 nm,
662 gain: 100) after a 15 min incubation at room temperature. The relative fluorescence units (RFU)
663 reported represent the fluorescence after the background fluorescence (WT spores, no terbium
664 chloride) has been subtracted. Data shown are the average fluorescence measured from three
665 independent spore purifications.
666
667 **Spore viability following heat treatment**
668 Spore viability after heat treatment was determined essentially as described in (35). Briefly, 1.75
669 OD_{600} equivalents of spores, or ~5 x 10^7 spores, were suspended in 500 µL sterile water.
670 Spores were aliquoted into 7 tubes and incubated at 37˚C (no heat), 50˚C, 60˚C, 65˚C, 70˚C,
671 75˚C, or 80˚C for 15 minutes. After incubation, spores were serially diluted into 1x PBS and the
672 dilutions were plated onto BHIS with taurocholate agar media. After overnight incubation,
673 colonies were enumerated to determine the number of germinated spores. Data shown are the
674 averages from three independent spore purifications.
675
676 **Optical density (OD_{600})-based germination assay**
677 The germination kinetics of spores were analyzed by measuring OD_{600} of spores over time in a
678 microplate reader similarly to what was done in (28, 30). For all OD_{600} based kinetic assays,
679 about 0.17 OD_{600} equivalents of spores, or ~5 x 10^6 spores, per condition tested were
680 suspended in BHIS media or germination buffer (50 mM HEPES, 100 mM NaCl, pH 7.5).
681 Spores were aliquoted into wells of a clear, flat bottomed 96-well plate (Falcon) with either
682 calcium or glycine at indicated final concentrations to a final volume of 180 µL. As indicated, 20
683 µL of taurocholate (final concentration 0.2% (3.8 mM), 0.5% (9.5 mM), or 1% (19 mM) w/v) was
684 added. For the EGTA experiments, the germination buffer included 50 mM glycine, and 2 µL of
685 $CaCl_2$ and/or EGTA stock (100X solution relative to the final concentration) was included in the

686 20 µL taurocholate solution. The OD_{600} was measured at 37˚C every 3 minutes for 1 hour with
687 continuous linear shaking in a Synergy H1 microplate reader (Biotek). All germinant stocks
688 solutions were solubilized in water and filter sterilized; an initial 0.5 M EGTA stock was made in
689 0.1 N HCl. To measure germination kinetics in response to varying concentrations of
690 taurocholate, glycine, or calcium, germinant solutions were serially diluted in sterile water before
691 being mixed with spores in a 96-well plate. The change in OD_{600} was calculated as the ratio of
692 the OD_{600} at each time point to the OD_{600} at time zero. To calculate the average change in
693 OD_{600}/minute at various concentrations of taurocholate, glycine, or calcium, the period of
694 greatest change during the germination assay was first determined. For various concentrations
695 of taurocholate and calcium, the greatest change was between 0 and 6 minutes and for various
696 concentrations of glycine, the greatest change was between 0 and 15 minutes. To calculate the
697 average change in OD_{600}/min, the OD_{600} from the start of this time period was subtracted from
698 the OD_{600} at the end of the time period and divided by the time (in minutes) of the period of
699 greatest change. Data shown for all OD_{600} based kinetic assays are averages from experiments
700 performed on three independent spore purifications.
701
702 **SleC cleavage analysis**
703 Spores were diluted to about 0.35 OD_{600} equivalents per time point tested (0.7 OD units total)
704 into germination buffer (50 mM HEPES, 100 mM NaCl, pH 7.5) with 50 mM glycine. One third of
705 the spore volume was removed as a starting time point control. Taurocholate (TA) was added to
706 the remaining two thirds spore volume to a final concentration of 0.2% (3.8 mM) w/v. Spores
707 were incubated at 37˚C and 100 µL samples were taken at 30- and 60-minutes post TA
708 addition. Samples were centrifuged to pellet spores and supernatant was removed. Spores
709 were resuspended into 50 µL EBB buffer (8 M urea, 2 M thiourea, 4% (w/v) SDS, 2% (v/v) β-
710 mercaptoethanol) for further analysis by western blotting.
711
712 **Western blot analysis**
713 Spore samples in EBB from SleC cleavage assays were boiled for 20 minutes with vortex
714 mixing and 4X NuPAGE LDS Sample Buffer (Thermo Fisher) was added to stain samples with
715 bromophenol blue. Samples were boiled for an additional 5-10 minutes with vortex mixing after
716 the addition of sample buffer. Samples were resolved by electrophoresis on a 12% SDS-PAGE
717 gel and transferred to a Millipore-Immobilon PVDF membrane for western blot analysis.
718 Membranes were blocked with a 1:1 dilution of Odyssey Blocking Buffer and 1X phosphate
719 buffered saline (PBS) with 0.1% (v/v) Tween 20 and probed with rabbit polyclonal anti-CotA

720 antibodies (50) and monoclonal mouse anti-SleC antibodies (27). The anti-CotA antibody was
721 used at a 1:1000 dilution and the anti-SleC antibody was used at a 1:5000 dilution. IRDye
722 680CV and 800CW infrared dye-conjugated secondary antibodies were used at 1:20,000
723 dilutions. Secondary antibody fluorescence emissions were detected on an Odyssey LiCor Clx.
724 Results shown are representative Western blot analyses from three independent spore
725 isolations.
726
727 **Phase-contrast microscopy analyses of spore hydration**
728 Spores were diluted to about 0.35 OD_{600} into germination buffer (50 mM HEPES, 100 mM NaCl,
729 pH 7.5). Spores were further diluted 1:5 in sterile water and 1.5 µL was added to an agarose
730 pad on a microscope slide and covered with a cover slip for analysis by phase-contrast
731 microscopy. Agarose pads were made by adhering a Gene Frame (ThermoFisher Scientific) to
732 a glass slide and filling the Gene Frame with 1%, 19 mM (w/v) agarose in germination buffer.
733 Agarose pads were incubated at 4˚C to solidify. Spores were analyzed on an Axioskop (Carl
734 Zeiss, West-Germany) upright microscope, a 100x 1.3 NA Plan NeoFluar phase contrast
735 objective, and images were taken using a Hamamatsu C4742-95 Orca 100 CCD Camera with a
736 25 ms exposure. Images were taken of fields with well-separated spores to ensure better
737 identification of spores in downstream analysis. Phase-contrast images were analyzed using the
738 MicrobeJ plug-in (44) for ImageJ to identify individual spores and measure the intensity of
739 phase-bright spore core. MicrobeJ analysis was completed with the following parameters: width
740 [p]: 0.6-1, circularity [0-1]: 0.5-1, curvature [0-max]: 0-0.4, sinuosity [0-max]:0-1.1, angularity
741 [rad]: 0-0.5, solidity [0-max]: 0-max, intensity [0-max]: 0-200, Z-score: 0-max, feature [0-max]: 0-
742 max, poles [0-max]: 0-max, range [p]: 0-max, symmetry: 0-max, holes [0-max]: 0-0. The percent
743 of spores correctly identified in an image varied between images and *C. difficile* strains, but at
744 least 275 spores were analyzed per strain in a replicate experiment. The average intensity (AU)
745 of individual spores was graphed as a proxy for spore hydration. The data shown derive from
746 three independent spore isolations.
747
748 **Single spore germination analyses**
749 <u>PySpore Validation Experiments</u>
750 To generate agarose pads for the analyses, 2X BHIS containing 1%, 19 mM TA was mixed with
751 molten 3.5% (w/v) Top-Vision Low Melting Point Agarose in sterile H_2O to a final concentration
752 of 1.75% agarose and 0.5% (9.5 mM) TA. The resulting media was added to a 125 µL gene-
753 frame (Thermo-Fisher Scientific) adhered to a clean glass microscope slide and solidified. WT,

754 Δ*pdaA,* and Δ*cwlD* spores were diluted to 0.2-0.5 OD_{600} in sterile H_2O in biological triplicate and
755 1µl was spotted on to a #1.5 coverslip and allowed to dry at 37˚C. After the spores dried, the
756 coverslip was inverted onto the agar pad and imaged immediately imaged via time-lapse phase-
757 contrast microscopy at 37˚C.
758
759 Glycine and Calcium Experiments
760 Agarose pads were made containing germination buffer (50 mM HEPES, 100 mM NaCl, pH
761 7.5), 1.75% (w/v) Top-Vision Low Melting Point Agarose, 0.2% (3.8 mM) TA (w/v), and either 10
762 mM Gly or 30 mM $CaCl_2$. The resulting media was added to a 125µl gene-frame (Thermo-Fisher
763 Scientific) adhered to a clean glass microscope slide and solidified. WT, Δ*dpaAB* spores were
764 diluted to 0.2-0.5 OD_{600} in sterile H_2O in biological triplicate and 1µl was spotted on to a #1.5
765 coverslip and allowed to dry at 37˚C. After the spores dried, the coverslip was inverted onto the
766 agar pad and imaged immediately imaged via time-lapse phase-contrast microscopy at 37˚C.
767
768 Spore Exudate Experiments
769 To generate the germination exudates used to make the agarose pads for analyzing spore
770 germination using time-lapse microscopy, the equivalent of 0.7 OD_{600} units were diluted into
771 germination buffer (50 mM HEPES, 100 mM NaCl, pH 7.5). The TA germinant and glycine co-
772 germinant were added to final concentrations of 0.5%, 9.5 mM TA and 2.5 mM glycine and
773 incubated at 37˚C for 4 hours. The germination exudate was harvested from the spores by
774 centrifuging the samples at 15,000 rpm for 2 minutes to pellet the spores and removing the
775 supernatant (i.e. the germination exudate). The supernatant/ exudate was centrifuged again at
776 15,000 rpm for 2 minutes. If the germination exudate was not immediately used, it was stored at
777 4˚C. Otherwise, the supernatant was incubated for ~10 minutes at 37˚C and then 200 µL of the
778 exudate was added to 100 µL of melted 3.3% agarose in germination buffer (50 mM HEPES,
779 100 mM NaCl, pH 7.5) for final concentration of 1% agarose. For the Ca^{2+} "add-back"
780 experiment, $CaCl_2$ added to a final concentration of 190 µM during the pre-warming step at
781 37˚C. The agarose-germination exudate solution was gently vortexed and then added to a Gene
782 Frame adhered to a microscope slide. The agarose pad was incubated at 4˚C to solidify the
783 agarose pad during which time 0.175 OD_{600} equivalents of WT spores were diluted 1:4 in sterile
784 water and vigorously pipetted to break up spore clumps. 1.5 µL of this WT spore mixture were
785 added to agarose pad; the pad was then sealed with a cover slip and immediately analyzed by
786 phase-contrast time-lapse microscopy.
787

788 Data Analysis
789 Resulting image stacks were registered if significant drift of the FOV was encountered,
790 segmented, and quantified using a custom GUI based Python application developed in-house
791 called PySpore. PySpore utilizes phase cross correlation for image registration/alignment of the
792 image stack. To segment spores a black-hat transform is applied to each image to enhance the
793 dark features of the spore, namely the spore coat, while also eliminating background and
794 correcting for discrepancies in illumination over the field. A threshold is chosen from the black-
795 hat processed image and a segmentation mask is generated. Each ROI then undergoes a
796 simple pixel overlap based image processing algorithm to track its position throughout the movie
797 and correct any discrepancies in spore ID, and measurements are extracted including size,
798 shape, and intensity from the phase-contrast images and are output as a .csv file for
799 downstream analysis.
800
801 All downstream analyses including statistical tests were done in Python. Spore clumps were
802 excluded based on area; spores tracked for less than 50 frames were also excluded from further
803 analysis. Additionally, highly noisy traces were excluded after evaluating the coefficient of
804 variation (CV) at multiple windows for each time series and discarded based on a threshold CV
805 value and the number of times that was exceeded in the time series.
806
807 Germination rate and time to germination were quantified from spores where germination was
808 tracked (>20% decrease in intensity from start to end). Maximal germination rate was
809 determined by evaluating the first derivative of 1-D smoothing spline fit to the data at each time
810 point. Time to germination was defined as the time point when the max germination rate is
811 reached.
812
813 PySpore code is available here: https://github.com/jribis89/PySpore
814
815 Microscope Hardware
816 Images were taken every 30 seconds using a Leica DMi8 inverted microscope equipped with a
817 63x 1.4NA Plan Apochromat phase-contrast objective, Leica Adaptive Focus Control (AFC), a
818 high precision motorized stage (Pecon), an incubator (Pecon), and a Leica DFC9000-GTC
819 sCMOS camera for all time-lapse analyses.
820
821 **References**

822

823 1. Desai K, Gupta SB, Dubberke ER, Prabhu VS, Browne C, Mast TC. 2016. Epidemiological
824 and economic burden of *Clostridium difficile* in the United States: estimates from a
825 modeling approach. BMC Infect Dis 16:303.
826 2. Guh AY, Mu Y, Winston LG, Johnston H, Olson D, Farley MM, Wilson LE, Holzbauer SM,
827 Phipps EC, Dumyati GK, Beldavs ZG, Kainer MA, Karlsson M, Gerding DN, McDonald LC,
828 Emerging Infections Program *Clostridioides difficile* Infection Working G. 2020. Trends in
829 U.S. Burden of Clostridioides difficile Infection and Outcomes. N Engl J Med 382:1320-
830 1330.
831 3. Abt MC, McKenney PT, Pamer EG. 2016. *Clostridium difficile* colitis: pathogenesis and host
832 defence. Nat Rev Microbiol doi:10.1038/nrmicro.2016.108.
833 4. Theriot CM, Young VB. 2015. Interactions Between the Gastrointestinal Microbiome and
834 *Clostridium difficile*. Annu Rev Microbiol 69:445-61.
835 5. Kordus SL, Thomas AK, Lacy DB. 2022. *Clostridioides difficile* toxins: mechanisms of
836 action and antitoxin therapeutics. Nat Rev Microbiol 20:285-298.
837 6. Deakin LJ, Clare S, Fagan RP, Dawson LF, Pickard DJ, West MR, Wren BW, Fairweather
838 NF, Dougan G, Lawley TD. 2012. The *Clostridium difficile spo0A* gene is a persistence and
839 transmission factor. Infect Immun 80:2704-11.
840 7. Lim SC, Hain-Saunders NMR, Imwattana K, Putsathit P, Collins DA, Riley TV. 2022.
841 Genetically related *Clostridium difficile* from water sources and human CDI cases revealed
842 by whole-genome sequencing. Environ Microbiol 24:1221-1230.
843 8. Lim SC, Knight DR, Riley TV. 2020. Clostridium difficile and One Health. Clin Microbiol
844 Infect 26:857-863.
845 9. Lawley T, Clare S, Deakin L, Goulding D, Yen J, Raisen C, Brandt C, Lovell J, Cooke F,
846 Clark T, Dougan G. 2010. Use of purified *Clostridium difficile* spores to facilitate evaluation
847 of health care disinfection regimens. Applied Environ Micrb 76:6895-6900.
848 10. Shen A. 2020. Clostridioides difficile Spores: Bile Acid Sensors and Trojan Horses of
849 Transmission. Clin Colon Rectal Surg 33:58-66.
850 11. Baloh M, Sorg JA. 2022. *Clostridioides difficile* spore germination: initiation to DPA release.
851 Curr Opin Microbiol 65:101-107.
852 12. Kochan TJ, Foley MH, Shoshiev MS, Somers MJ, Carlson PE, Hanna PC. 2018. Updates
853 to *Clostridium difficile* Spore Germination. J Bacteriol 200.
854 13. Shen A. 2020. *Clostridioides difficile* Spore Formation and Germination: New Insights and
855 Opportunities for Intervention. Annu Rev Microbiol 74:545-566.
856 14. Howerton A, Patra M, Abel-Santos E. 2013. A new strategy for the prevention of
857 *Clostridium difficile i*nfection. J Infect Dis 207:1498-504.
858 15. Shen A, Edwards AN, Sarker MR, Paredes-Sabja D. 2019. Sporulation and Germination in
859 Clostridial Pathogens. Microbiol Spectr 7.
860 16. Paredes-Sabja D, Setlow P, Sarker M. 2011. Germination of spores of Bacillales and
861 Clostridiales species: mechanisms and proteins involved. Trends Micrb 19:85-94.
862 17. Artzi L, Alon A, Brock KP, Green AG, Tam A, Ramirez-Guadiana FH, Marks D, Kruse A,
863 Rudner DZ. 2021. Dormant spores sense amino acids through the B subunits of their
864 germination receptors. Nat Commun 12:6842.
865 18. Setlow P, Wang S, Li YQ. 2017. Germination of Spores of the Orders Bacillales and
866 Clostridiales. Annu Rev Microbiol 71:459-477.
867 19. Galperin MY, Yutin N, Wolf YI, Vera Alvarez R, Koonin EV. 2022. Conservation and
868 Evolution of the Sporulation Gene Set in Diverse Members of the Firmicutes. J Bacteriol
869 204:e0007922.

870 20. Francis MB, Allen CA, Shrestha R, Sorg JA. 2013. Bile acid recognition by the *Clostridium*
871 *difficile* germinant receptor, CspC, is important for establishing infection. PLoS Pathog
872 9:e1003356.
873 21. Ridlon JM, Kang DJ, Hylemon PB. 2006. Bile salt biotransformations by human intestinal
874 bacteria. J Lipid Res 47:241-59.
875 22. Guzior DV, Quinn RA. 2021. Review: microbial transformations of human bile acids.
876 Microbiome 9:140.
877 23. Sorg JA, Sonenshein AL. 2008. Bile salts and glycine as cogerminants for *Clostridium*
878 *difficile* spores. J Bacteriol 190:2505-12.
879 24. Kochan TJ, Somers MJ, Kaiser AM, Shoshiev MS, Hagan AK, Hastie JL, Giordano NP,
880 Smith AD, Schubert AM, Carlson PE, Jr., Hanna PC. 2017. Intestinal calcium and bile salts
881 facilitate germination of Clostridium difficile spores. PLoS Pathog 13:e1006443.
882 25. Shrestha R, Sorg JA. 2018. Hierarchical recognition of amino acid co-germinants during
883 Clostridioides difficile spore germination. Anaerobe 49:41-47.
884 26. Shrestha R, Sorg JA. 2019. Terbium chloride influences *Clostridium difficile* spore
885 germination. Anaerobe 58:80-88.
886 27. Adams CM, Eckenroth BE, Putnam EE, Doublie S, Shen A. 2013. Structural and functional
887 analysis of the CspB protease required for *Clostridium* spore germination. PLoS Pathog
888 9:e1003165.
889 28. Shrestha R, Cochran AM, Sorg JA. 2019. The requirement for co-germinants during
890 *Clostridium difficile* spore germination is influenced by mutations in *yabG* and *cspA*. PLoS
891 Pathog 15:e1007681.
892 29. Kevorkian Y, Shirley DJ, Shen A. 2016. Regulation of *Clostridium difficile* spore germination
893 by the CspA pseudoprotease domain. Biochimie 122:243-54.
894 30. Rohlfing AE, Eckenroth BE, Forster ER, Kevorkian Y, Donnelly ML, Benito de la Puebla H,
895 Doublie S, Shen A. 2019. The CspC pseudoprotease regulates germination of
896 *Clostridioides difficile* spores in response to multiple environmental signals. PLoS Genet
897 15:e1008224.
898 31. Francis MB, Allen CA, Sorg JA. 2015. Spore cortex hydrolysis precedes DPA release
899 during *Clostridium difficile* spore germination. J Bacteriol doi:10.1128/JB.02575-14.
900 32. Francis MB, Sorg JA. 2016. Dipicolinic Acid Release by Germinating *Clostridium difficile*
901 Spores Occurs through a Mechanosensing Mechanism. mSphere 1.
902 33. Velasquez J, Schuurman-Wolters G, Birkner JP, Abee T, Poolman B. 2014. *Bacillus subtilis*
903 spore protein SpoVAC functions as a mechanosensitive channel. Mol Microbiol 92:813-23.
904 34. Wang S, Shen A, Setlow P, Li YQ. 2015. Characterization of the dynamic germination of
905 individual *Clostridium difficile* spores using Raman spectroscopy and differential
906 interference contrast microscopy. J Bacteriol doi:10.1128/JB.00200-15.
907 35. Donnelly ML, Fimlaid KA, Shen A. 2016. Characterization of *Clostridium difficile* Spores
908 Lacking Either SpoVAC or Dipicolinic Acid Synthetase. J Bacteriol 198:1694-1707.
909 36. Daniel RA, Errington J. 1993. Cloning, DNA sequence, functional analysis and
910 transcriptional regulation of the genes encoding dipicolinic acid synthetase required for
911 sporulation in *Bacillus subtilis*. J Mol Biol 232:468-83.
912 37. Ramirez-Guadiana FH, Meeske AJ, Rodrigues CDA, Barajas-Ornelas RDC, Kruse AC,
913 Rudner DZ. 2017. A two-step transport pathway allows the mother cell to nurture the
914 developing spore in *Bacillus subtilis*. PLoS Genet 13:e1007015.
915 38. Vepachedu VR, Setlow P. 2007. Role of SpoVA proteins in release of dipicolinic acid during
916 germination of *Bacillus subtilis* spores triggered by dodecylamine or lysozyme. J Bacteriol
917 189:1565-72.
918 39. Paredes-Sabja D, Setlow B, Setlow P, Sarker MR. 2008. Characterization of *Clostridium*
919 *perfringens* spores that lack SpoVA proteins and dipicolinic acid. J Bacteriol 190:4648-59.

920 40. Vepachedu VR, Setlow P. 2004. Analysis of the germination of spores of *Bacillus subtilis*
921 with temperature sensitive *spo* mutations in the *spoVA* operon. FEMS Microbiol Lett
922 239:71-7.
923 41. Tovar-Rojo F, Chander M, Setlow B, Setlow P. 2002. The products of the *spoVA* operon
924 are involved in dipicolinic acid uptake into developing spores of *Bacillus subtilis*. J Bacteriol
925 184:584-7.
926 42. Berendsen EM, Koning RA, Boekhorst J, de Jong A, Kuipers OP, Wells-Bennik MH. 2016.
927 High-Level Heat Resistance of Spores of *Bacillus amyloliquefaciens* and B*acillus*
928 *licheniformis* Results from the Presence of a *spoVA* Operon in a Tn1546 Transposon. Front
929 Microbiol 7:1912.
930 43. Gao Y, Barajas-Ornelas RDC, Amon JD, Ramirez-Guadiana FH, Alon A, Brock KP, Marks
931 DS, Kruse AC, Rudner DZ. 2022. The SpoVA membrane complex is required for dipicolinic
932 acid import during sporulation and export during germination. Genes Dev 36:634-646.
933 44. Ducret A, Quardokus EM, Brun YV. 2016. MicrobeJ, a tool for high throughput bacterial cell
934 detection and quantitative analysis. Nat Microbiol 1:16077.
935 45. Hindle AA, Hall EA. 1999. Dipicolinic acid (DPA) assay revisited and appraised for spore
936 detection. Analyst 124:1599-604.
937 46. Kong L, Zhang P, Setlow P, Li YQ. 2010. Characterization of bacterial spore germination
938 using integrated phase contrast microscopy, Raman spectroscopy, and optical tweezers.
939 Anal Chem 82:3840-7.
940 47. Sunde EP, Setlow P, Hederstedt L, Halle B. 2009. The physical state of water in bacterial
941 spores. Proc Natl Acad Sci U S A 106:19334-9.
942 48. Beaman TC, Greenamyre JT, Corner TR, Pankratz HS, Gerhardt P. 1982. Bacterial spore
943 heat resistance correlated with water content, wet density, and protoplast/sporoplast
944 volume ratio. J Bacteriol 150:870-7.
945 49. Paidhungat M, Setlow B, Driks A, Setlow P. 2000. Characterization of spores of *Bacillus*
946 *subtilis* which lack dipicolinic acid. J Bacteriol 182:5505-12.
947 50. Donnelly ML, Li W, Li YQ, Hinkel L, Setlow P, Shen A. 2017. A *Clostridium difficile*-Specific,
948 Gel-Forming Protein Required for Optimal Spore Germination. mBio 8.
949 51. Diaz OR, Sayer CV, Popham DL, Shen A. 2018. *Clostridium difficile* Lipoprotein GerS Is
950 Required for Cortex Modification and Thus Spore Germination. mSphere 3.
951 52. Pandey R, Ter Beek A, Vischer NO, Smelt JP, Brul S, Manders EM. 2013. Live cell imaging
952 of germination and outgrowth of individual *Bacillus subtilis* spores; the effect of heat stress
953 quantitatively analyzed with SporeTracker. PLoS One 8:e58972.
954 53. Kong L, Zhang P, Wang G, Yu J, Setlow P, Li YQ. 2011. Characterization of bacterial spore
955 germination using phase-contrast and fluorescence microscopy, Raman spectroscopy and
956 optical tweezers. Nat Protoc 6:625-39.
957 54. Coullon H, Rifflet A, Wheeler R, Janoir C, Boneca IG, Candela T. 2018. N-Deacetylases
958 required for muramic-delta-lactam production are involved in *Clostridium difficile*
959 sporulation, germination, and heat resistance. J Biol Chem 293:18040-18054.
960 55. Leslie JL, Jenior ML, Vendrov KC, Standke AK, Barron MR, O'Brien TJ, Unverdorben L,
961 Thaprawat P, Bergin IL, Schloss PD, Young VB. 2021. Protection from Lethal *Clostridioides*
962 *difficile* Infection via Intraspecies Competition for Cogerminant. mBio 12.
963 56. Ng YK, Ehsaan M, Philip S, Collery MM, Janoir C, Collignon A, Cartman ST, Minton NP.
964 2013. Expanding the repertoire of gene tools for precise manipulation of the *Clostridium*
965 *difficile* genome: allelic exchange using pyrE alleles. PLoS One 8:e56051.
966 57. Karasawa T, Ikoma S, Yamakawa K, Nakamura S. 1995. A defined growth medium for
967 *Clostridium difficile*. Microbiology 141:371-5.
968 58. Ribis JW, Ravichandran P, Putnam EE, Pishdadian K, Shen A. 2017. The Conserved
969 Spore Coat Protein SpoVM Is Largely Dispensable in *Clostridium difficile* Spore Formation.
970 mSphere 2.

974 **Figure Legends**

975

976 **Figure 1. Mutants with defects in storing CaDPA in their core are more hydrated and less**
977 **heat-resistant**. (A) Schematic of CaDPA synthesis and transport during spore formation in *C.*
978 *difficile*. DpaAB is the enzymatic complex that synthesizes DPA, which complexes with Ca^{2+}
979 ions before it is transported across the outer (OM) and inner forespore membranes (IM). SpoVV
980 is the putative CaDPA transporter in the OM (37), while SpoVAC is the CaDPA transporter
981 located in the IM (43). CD3298 (orange circle) is a putative ATP-binding protein previously
982 shown to be important for CaDPA transport in *C. difficile* (24), but it is unclear whether it
983 associates with SpoVV or SpoVAC. (B) CaDPA levels measured in spores purified from WT,
984 Δ*spoVV*, Δ*dpaAB*, Δ*cd3298*, Δ*spoVAC*, and their respective complementation strains. CaDPA
985 levels were measured using terbium fluorescence after spores were boiled to release CaDPA or
986 left untreated (RFU = relative fluorescent units). The average CaDPA measured on three
987 independent spore preparations and associated standard deviation are shown. (C) SuperPlot
988 comparison of CaDPA mutant spore intensity as measured by phase-contrast microscopy. The
989 intensity of spores purified from the indicated strains was determined by phase-contrast
990 microscopy using the MicrobeJ Fiji plug-in (44). A minimum of 650 spores was analyzed for
991 each strain; the mean intensity for a given biological replicate is shown as large dots; the
992 horizontal line represents the average of the mean intensity value for the three biological
993 replicates. Statistical significance was determined using one-way ANOVA and Tukey's test. (D)
994 Optical density (OD_{600})-based analyses of spore germination over time in the indicated strains.
995 Germination was induced in the presence of rich media (BHIS) and 1% (19 mM) taurocholate.
996 The ratio of the OD_{600} of each strain at a given time point relative to the OD_{600} at time zero was
997 plotted. The average of three independent experiments using three independent spore
998 purifications is shown, and shaded error bars indicate the standard deviation for each time point
999 measured. Statistical significance relative to WT was determined using a two-way ANOVA and
1000 Tukey's test. **** $p < 0.0001$, *** $p < 0.001$, ** $p < 0.01$, * $p < 0.05$, n.s. = no statistical
1001 significance.

1002

1003

1004 **Figure 2. CaDPA mutant spores germinate in response to either Ca^{2+} or glycine co-**
1005 **germinants**. Optical density (OD_{600})-based analyses of spore germination over time in the
1006 presence of the indicated concentrations of taurocholate and either glycine (A, C, D) or Ca^{2+} (B)
1007 co-germinants. The ratio of the OD_{600} of each strain at a given time point relative to at time zero

1008 was plotted. The average of three independent experiments (conducted on three independent
1009 spore purifications) is shown, and shaded error bars indicate the standard deviation for each
1010 time point measured. Statistical significance relative to WT was determined using a two-way
1011 ANOVA and Tukey's test. **** $p < 0.0001$, *** $p < 0.001$, ** $p < 0.01$. (E) Western blot analyses
1012 of SleC activation following 0.2% (3.8 mM) TA and 50 mM glycine exposure in the indicated
1013 strains. The pro-SleC zymogen is proteolytically activated by the CspB protease in response to
1014 TA germinant and co-germinant signals (27, 28). CotA was used as a loading control (50).
1015
1016 **Figure 3. Sensitivity of CaDPA mutant spores to Ca^{2+} co-germinant**. (A) Optical density
1017 (OD_{600})-based analyses of spore germination over time in the presence of the indicated
1018 concentrations of taurocholate and Ca^{2+}. The ratio of the OD_{600} of each strain at a given time
1019 point relative to at time zero was plotted. (B) Germination rate as a function of Ca^{2+} co-
1020 germinant concentration. Germination rate was defined as the average change in OD_{600} in the
1021 first 6 min of the assay. (C) Optical density (OD_{600})-based analyses of spore germination over
1022 time in the presence of the indicated concentrations of taurocholate and glycine. The average of
1023 three independent experiments (conducted on three independent spore purifications) is shown,
1024 and shaded error bars indicate the standard deviation for each time point measured. (D)
1025 Germination rate as a function of glycine co-germinant concentration. Germination rate was
1026 defined as the average change in OD_{600} in the first 15 min of the assay. For all the data in this
1027 figure, the average of three independent experiments conducted on three independent spore
1028 purifications is shown, and the shaded error bars indicate the standard deviation for each time
1029 point measured.
1030
1031 **Figure 4. PySpore Automated image analysis pipeline for quantifying single-spore**
1032 **germination kinetics using time-lapse microscopy analyses**. (A) Schematic of PySpore
1033 analyses of spore germination. Images from time-lapse microscopy are processed using a
1034 black-hat transform to identify spores based by enhancing their phase-dark outline. After spores
1035 are segmented, a simple single-particle tracking scheme allows them to be tracked throughout
1036 the course of the movie, and their intensities can be plotted over time. (B) Percent of germinated
1037 WT, Δ*cwlD*, Δ*pdaA*, and Δ*cspC* spores detected by the PySpore program for the indicated
1038 strains when spotted onto BHIS agarose pads containing 0.5%, 9.5 mM taurocholate. Spores
1039 whose intensity was below a specific threshold that did not change over time are included in the
1040 percent germinated value. Quantification of (C) time to germination and (D) maximum
1041 germination rate from PySpore analyses of the single-spore germination traces. (E) Single-

1042 spore germination traces of the change in relative intensity of WT, Δ*cwlD*, Δ*pdaA* spores. The
1043 ratio of the intensity at a given time point relative to the starting intensity is plotted. Statistical
1044 significance was determined via the Kruskal-Wallis test *p < 0.05. Blue points represent the
1045 median of each biological replicate, error bars show the mean (diamond) and standard error. (F)
1046 Filmstrip of time-lapse microscopy analyses of the indicated spores spotted on BHIS + 0.5%,
1047 9.5 mM TA agarose pads. Parts of this figure were created with BioRender.
1048
1049 **Figure 5 Single-spore analysis of the individual roles of Ca^{2+} and Gly during germination.**
1050 (A) Kinetic analysis of percent germination of WT and Δ*dpaAB* spores in HEPES-NaCl buffer
1051 containing 0.2% (3.8 mM) TA and 10 mM glycine or 30 mM $CaCl_2$. (B) Comparison of maximal
1052 germination rate for WT and Δ*dpaAB* with either glycine or calcium alone. (C) Single
1053 germination traces showing the change in intensity over time under each condition. (D)
1054 Filmstrips of WT and Δ*dpaAB* in each buffer condition (scale bar = 5 µm). Statistical significance
1055 was determined via the Kruskal-Wallis test * p < 0.05**.** Blue points represent the median of each
1056 biological replicate, error bars show the mean of all biological replicates (grey diamond) and
1057 standard error.
1058
1059 **Figure 6. Ca^{2+} released during WT spore germination can serve as a "public good" to**
1060 **potentiate the germination of neighboring spores**. (A) Schematic of germination exudate
1061 preparation. Phase-contrast microscopy images highlight the delayed germination kinetics of
1062 Δ*dpaAB* spores in the presence of low glycine and TA. After germinating WT and Δ*dpaAB*
1063 spores in 2.5 mM glycine and 0.5% (9.5 mM) TA, germination "exudates" were harvested by
1064 pelleting spores and removing the supernatant fraction. This fraction was incorporated into
1065 agarose pads, and the ability of CaDPA released into the WT germination exudate fraction to
1066 potentiate germination in "naïve" WT spores is assessed. (B) Percent of germinated spores
1067 detected by the PySpore program for the indicated strains when spotted onto BHIS agarose
1068 pads containing 0.5% (9.5 mM) taurocholate. Spores whose intensity was below a specific
1069 threshold that did not change over time are included in the percent germinated value. (C) Single
1070 spore traces showing the change in intensity over time for WT spores in the presence of each
1071 harvested exudate. (D) Filmstrips of germination for WT spores germinating in the presence of
1072 harvested exudates.
1073
1074 **Figure 7. Micromolar concentrations of Ca^{2+} appear to be required for *C. difficile***
1075 **germination to proceed.** Optical density (OD_{600})-based analyses of WT and Δ*dpaAB* spore

1076 germination over time in the presence of 0.2% (3.8 mM) taurocholate and 50 mM glycine and
1077 the indicated concentrations of EGTA (A) and 5 μM EGTA and/or 5 μM Ca^{2+} (B). The ratio of the
1078 OD_{600} of each strain at a given time point relative to at time zero was plotted. The average of
1079 three independent experiments (conducted on three independent spore purifications) is shown,
1080 and shaded error bars indicate the standard deviation for each time point measured. Statistical
1081 significance relative to the untreated sample was determined using a two-way ANOVA and
1082 Tukey's test.
1083
1084 **Supplementary Figure Legends**
1085
1086 **Figure S1. CaDPA mutant spores are less "phase-bright".**
1087
1088 **Figure S2**. **Spore purification efficiency and heat resistance of CaDPA mutant spores.**
1089
1090 **Figure S3. Spline determination of germination rate and germination time.**
1091
1092 **Figure S4. Comparison of PySpore and SporeTrackerX.**
1093
1094 **Figure S5. Comparison of CaDPA mutant spore germination in the presence of glycine vs.**
1095 **Ca^{2+} co-germinant**.
1096
1097 **Figure S6. Micromolar concentrations of Ca^{2+} appear to be required for *C. difficile***
1098 **germination to proceed**

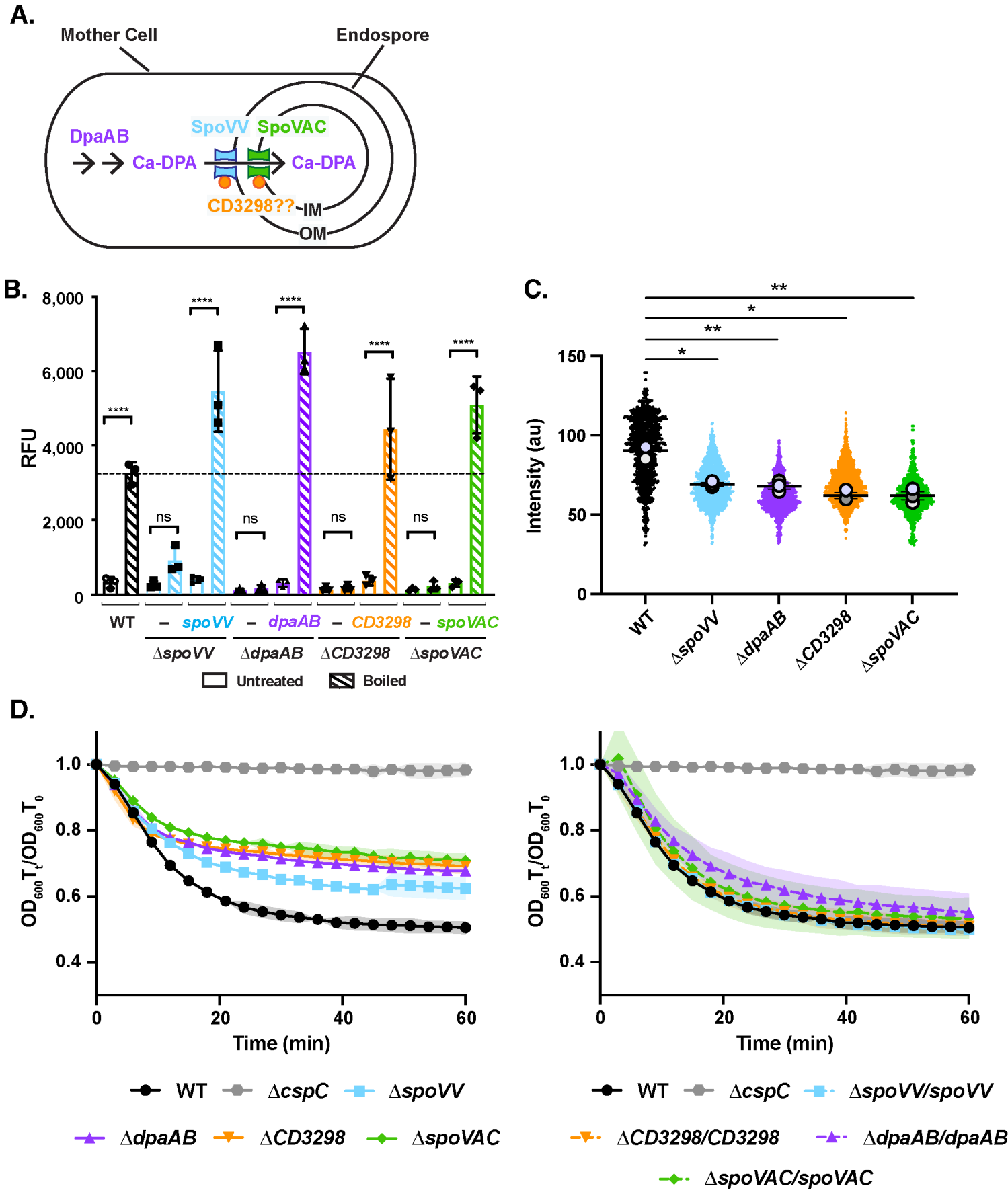
A.
Mother Cell
Endospore
DpaAB
Ca-DPA
SpoVV
SpoVAC
Ca-DPA
CD3298??
IM
OM
B.
RFU
8,000
6,000
4,000
2,000
0
****
ns
WT
– spoVV
– dpaAB
– CD3298
– spoVAC
ΔspoVV
ΔdpaAB
ΔCD3298
ΔspoVAC
Untreated
Boiled
C.
Intensity (au)
150
100
50
0
**
*
WT
ΔspoVV
ΔdpaAB
ΔCD3298
ΔspoVAC
D.
OD600 Tt/OD600 T0
1.0
0.8
0.6
0.4
0
20
40
60
Time (min)
WT
ΔcspC
ΔspoVV
ΔdpaAB
ΔCD3298
ΔspoVAC
ΔspoVV/spoVV
ΔCD3298/CD3298
ΔdpaAB/dpaAB
ΔspoVAC/spoVAC

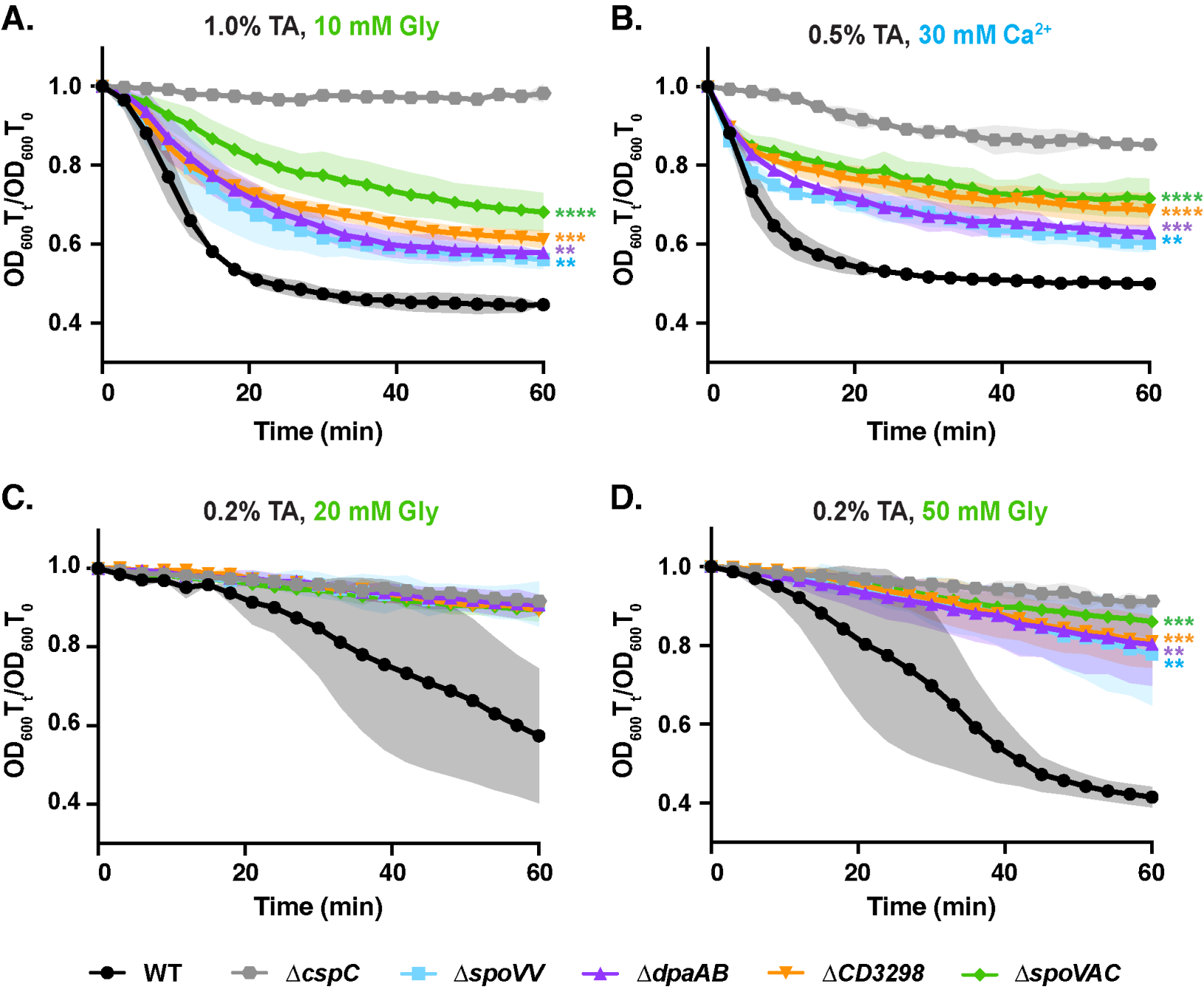
A.
1.0% TA, 10 mM Gly
B.
0.5% TA, 30 mM Ca2+
C.
0.2% TA, 20 mM Gly
D.
0.2% TA, 50 mM Gly
OD600Tt/OD600T0
Time (min)
****
***
**
WT
ΔcspC
ΔspoVV
ΔdpaAB
ΔCD3298
ΔspoVAC

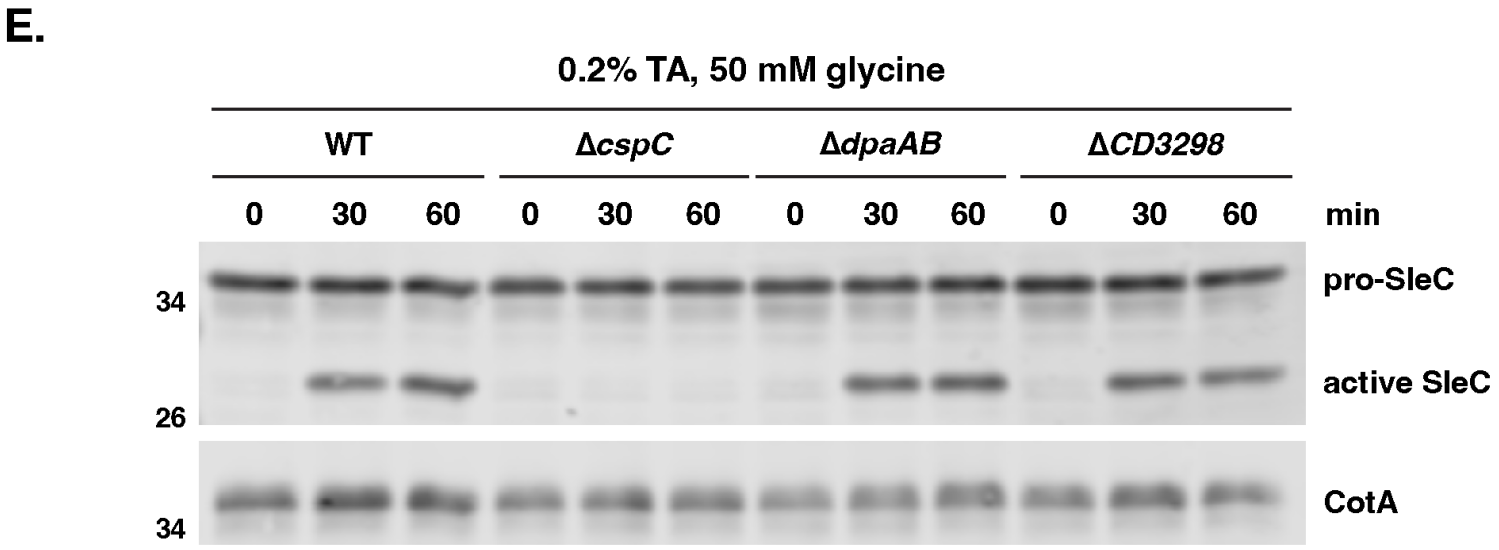
E.
0.2% TA, 50 mM glycine
WT
ΔcspC
ΔdpaAB
ΔCD3298
0 30 60 0 30 60 0 30 60 0 30 60
min
34
26
34
pro-SleC
active SleC
CotA

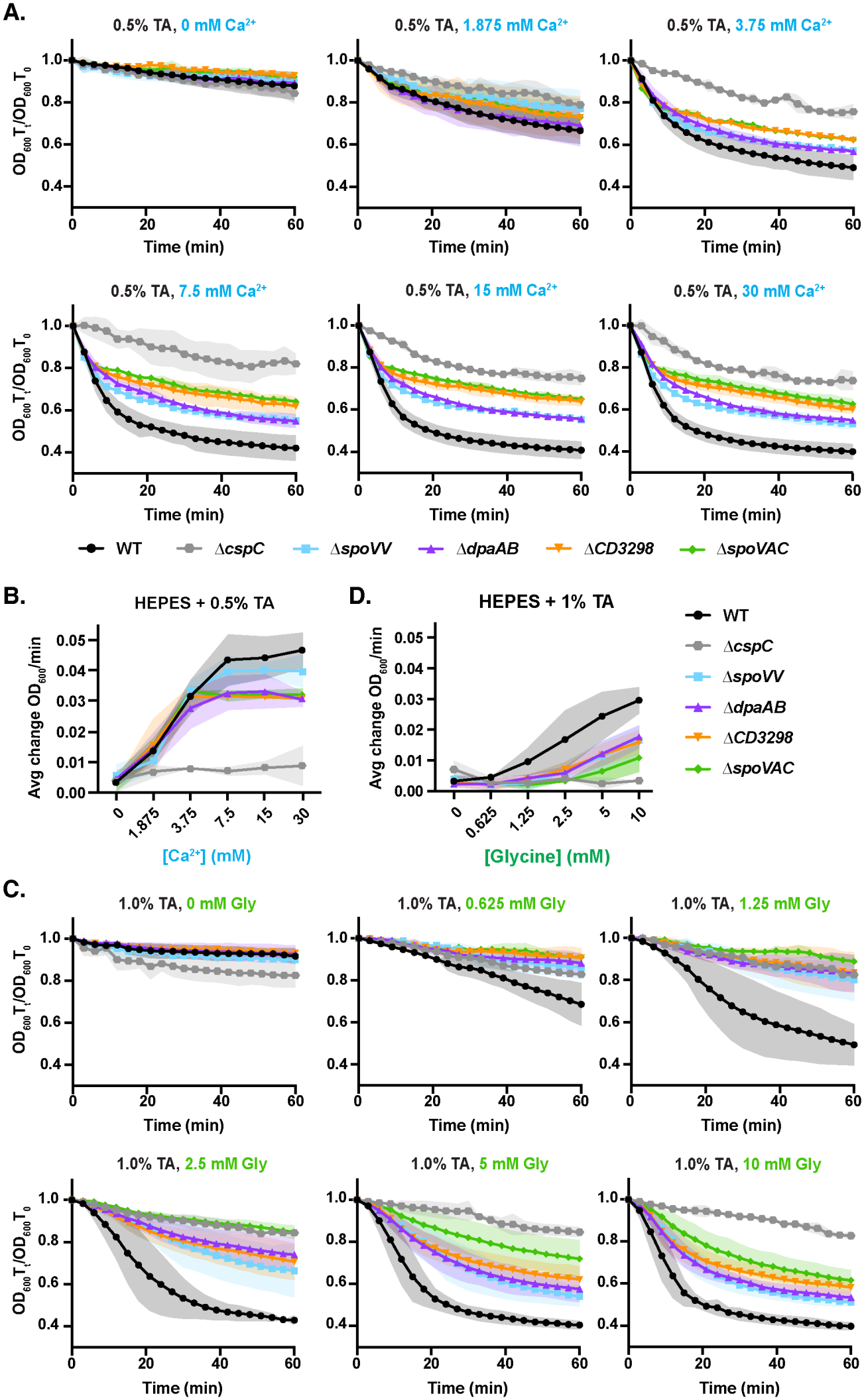
A.
0.5% TA, 0 mM Ca2+
0.5% TA, 1.875 mM Ca2+
0.5% TA, 3.75 mM Ca2+
0.5% TA, 7.5 mM Ca2+
0.5% TA, 15 mM Ca2+
0.5% TA, 30 mM Ca2+
OD600 Tt/OD600 T0
Time (min)
WT
ΔcspC
ΔspoVV
ΔdpaAB
ΔCD3298
ΔspoVAC
B.
HEPES + 0.5% TA
Avg change OD600/min
[Ca2+] (mM)
D.
HEPES + 1% TA
[Glycine] (mM)
C.
1.0% TA, 0 mM Gly
1.0% TA, 0.625 mM Gly
1.0% TA, 1.25 mM Gly
1.0% TA, 2.5 mM Gly
1.0% TA, 5 mM Gly
1.0% TA, 10 mM Gly

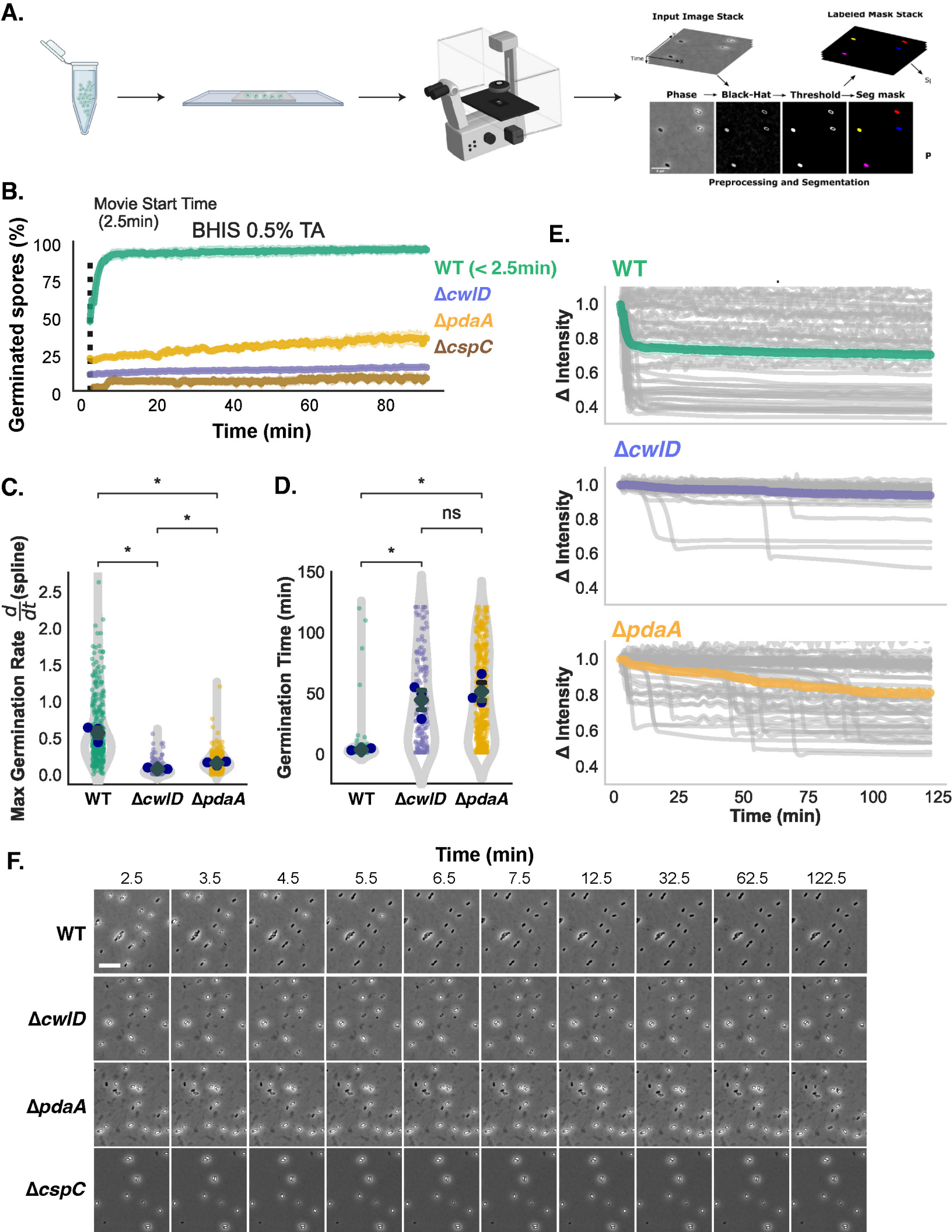
A.
Input Image Stack
Labeled Mask Stack
Phase
Black-Hat
Threshold
Seg mask
Preprocessing and Segmentation
B.
Movie Start Time
(2.5min)
BHIS 0.5% TA
Germinated spores (%)
Time (min)
WT (< 2.5min)
ΔcwlD
ΔpdaA
ΔcspC
C.
Max Germination Rate $\frac{d}{dt}$(spline)
WT
ΔcwlD
ΔpdaA
D.
Germination Time (min)
ns
E.
Δ Intensity
Time (min)
F.
Time (min)
2.5
3.5
4.5
5.5
6.5
7.5
12.5
32.5
62.5
122.5

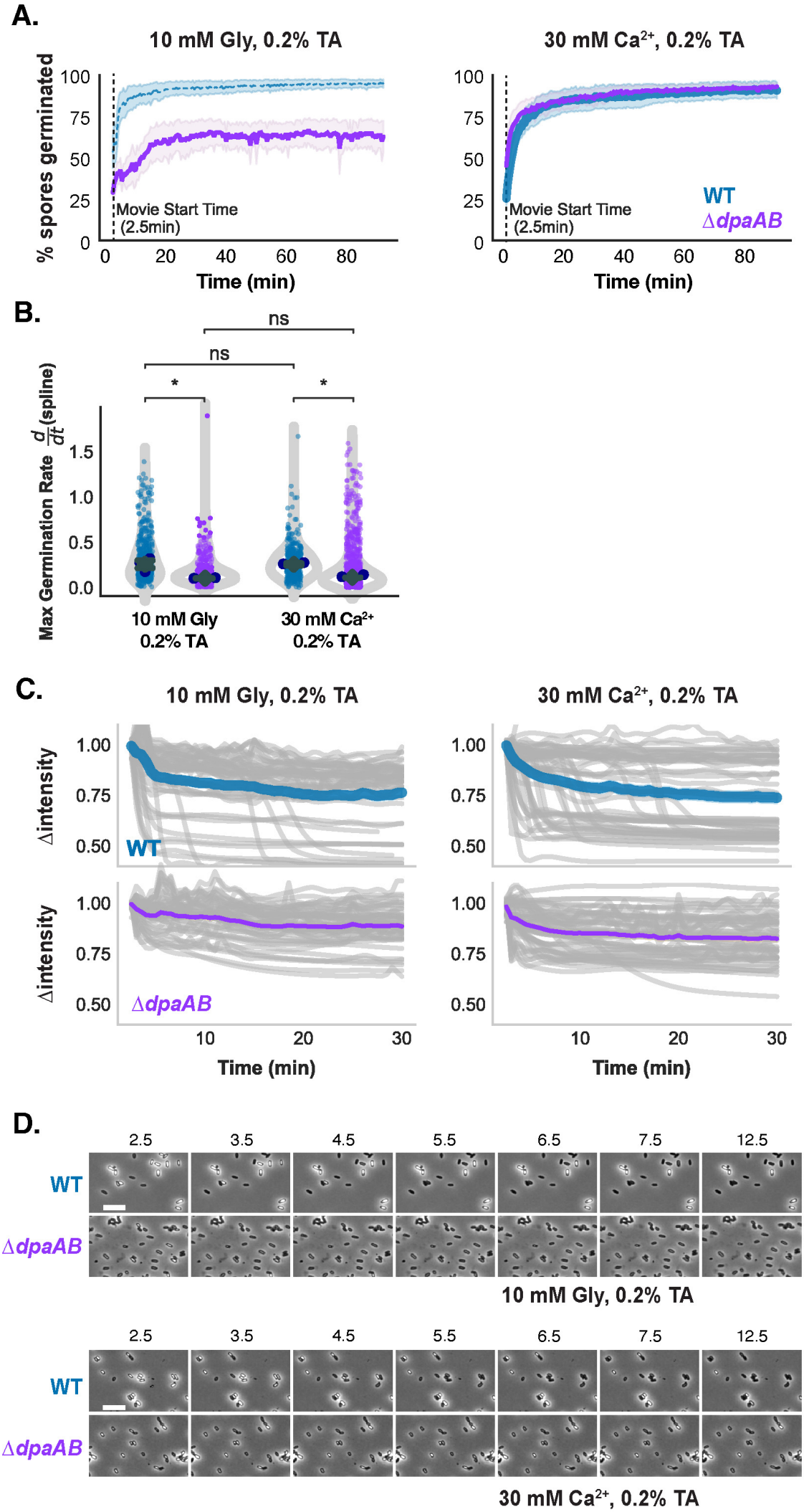
A.
10 mM Gly, 0.2% TA
30 mM Ca2+, 0.2% TA
% spores germinated
Movie Start Time
(2.5min)
Time (min)
WT
ΔdpaAB
B.
ns
ns
*
*
Max Germination Rate d/dt(spline)
10 mM Gly
0.2% TA
30 mM Ca2+
0.2% TA
C.
10 mM Gly, 0.2% TA
30 mM Ca2+, 0.2% TA
Δintensity
WT
ΔdpaAB
Time (min)
D.
2.5
3.5
4.5
5.5
6.5
7.5
12.5
17.5
32.5
92.5
WT
ΔdpaAB
10 mM Gly, 0.2% TA
30 mM Ca2+, 0.2% TA

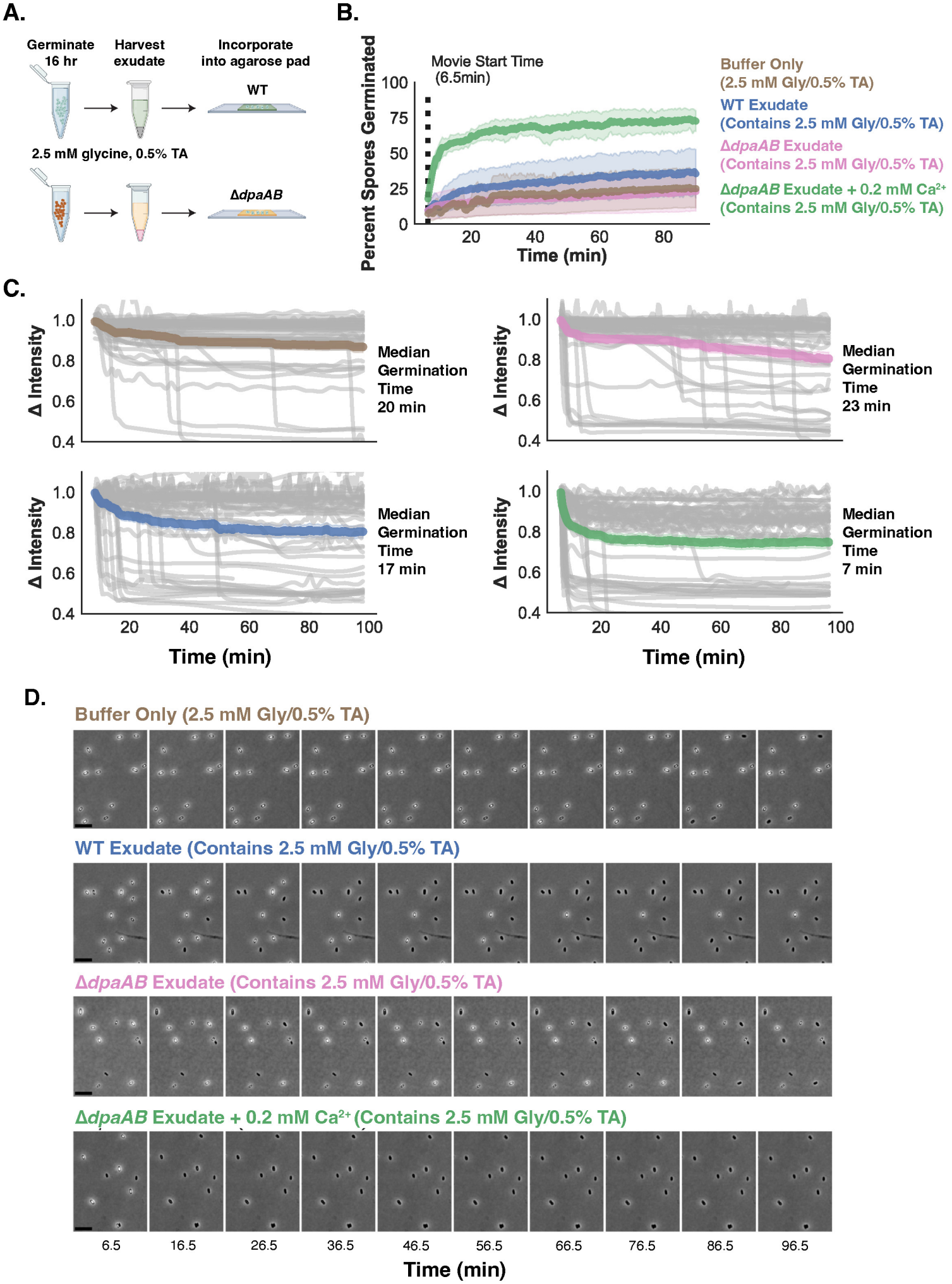
A.
Germinate 16 hr
Harvest exudate
Incorporate into agarose pad
WT
2.5 mM glycine, 0.5% TA
ΔdpaAB
B.
Movie Start Time (6.5min)
Percent Spores Germinated
Time (min)
Buffer Only (2.5 mM Gly/0.5% TA)
WT Exudate (Contains 2.5 mM Gly/0.5% TA)
ΔdpaAB Exudate (Contains 2.5 mM Gly/0.5% TA)
ΔdpaAB Exudate + 0.2 mM Ca2+ (Contains 2.5 mM Gly/0.5% TA)
C.
Δ Intensity
Median Germination Time 20 min
Median Germination Time 23 min
Median Germination Time 17 min
Median Germination Time 7 min
Time (min)
D.
Buffer Only (2.5 mM Gly/0.5% TA)
WT Exudate (Contains 2.5 mM Gly/0.5% TA)
ΔdpaAB Exudate (Contains 2.5 mM Gly/0.5% TA)
ΔdpaAB Exudate + 0.2 mM Ca2+ (Contains 2.5 mM Gly/0.5% TA)
6.5
16.5
26.5
36.5
46.5
56.5
66.5
76.5
86.5
96.5
Time (min)

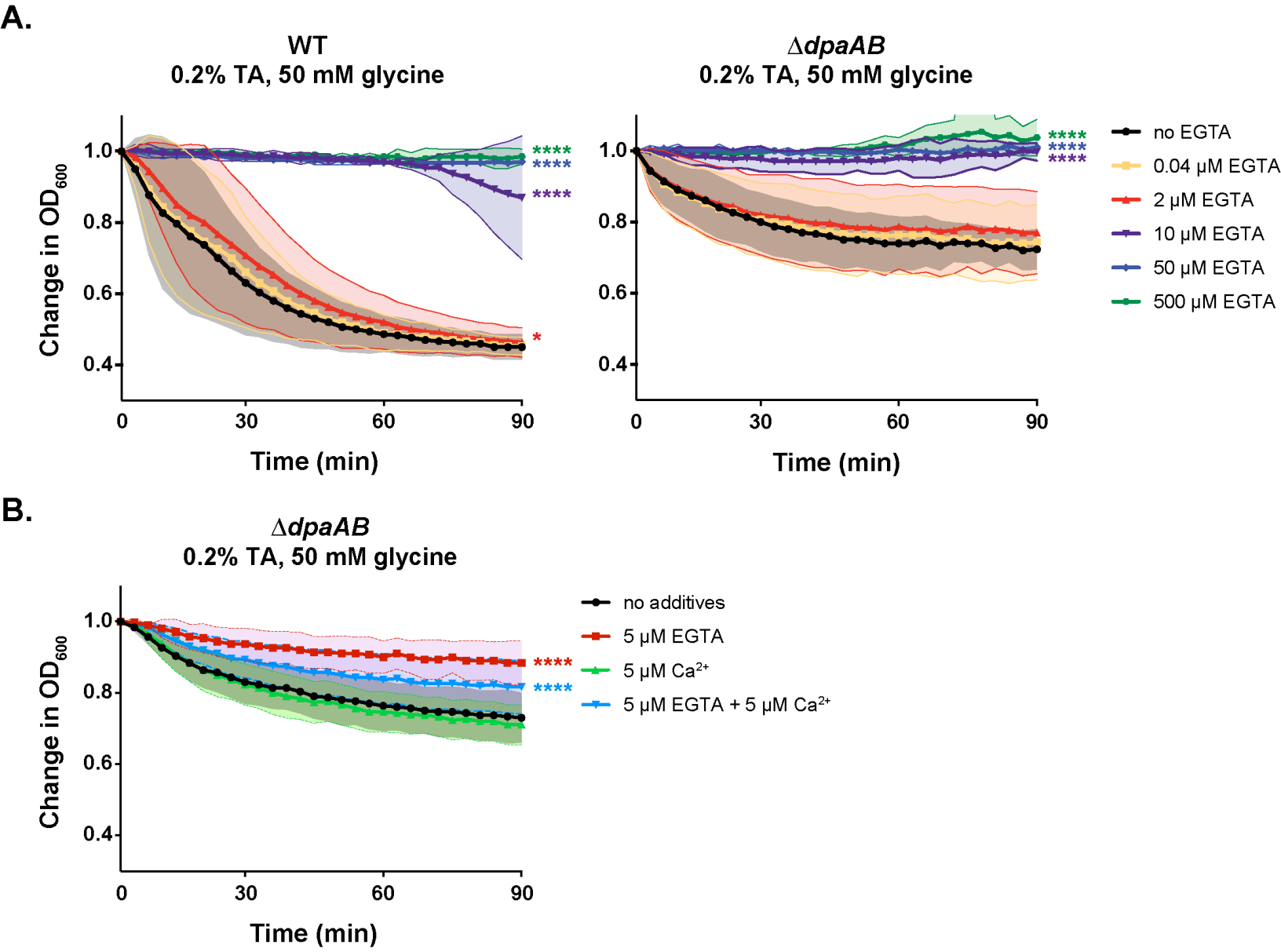
A.
WT
0.2% TA, 50 mM glycine
ΔdpaAB
0.2% TA, 50 mM glycine
Change in OD600
1.0
0.8
0.6
0.4
0
30
60
90
Time (min)
****
*
no EGTA
0.04 μM EGTA
2 μM EGTA
10 μM EGTA
50 μM EGTA
500 μM EGTA
B.
ΔdpaAB
0.2% TA, 50 mM glycine
no additives
5 μM EGTA
5 μM Ca2+
5 μM EGTA + 5 μM Ca2+